# REPORT DOCUMENTATION PAGE

Form Approved OMB NO. 0704-0188



| 1. REPORT DATE (DD-MM-YYYY) | 2. REPORT TYPE | 3. DATES COVERED (From - To) |
|---|---|---|
| 23-06-2010 | Final Report | 15-Jun-2007 - 14-Jul-2008 |

4. TITLE AND SUBTITLE
High Speed Imaging using Nanoprobe Arrays

5a. CONTRACT NUMBER
W911NF-07-1-0390

5b. GRANT NUMBER

5c. PROGRAM ELEMENT NUMBER
7310AI

6. AUTHORS
William P. King

5d. PROJECT NUMBER

5e. TASK NUMBER

5f. WORK UNIT NUMBER

7. PERFORMING ORGANIZATION NAMES AND ADDRESSES
University of Illinois - Urbana - Champaign
BOARD OF TRUSTEES OF THE UNIVERSITY OF ILLIN
1901 S. First Street, Suite A
Champaign, IL 61820 -7406

8. PERFORMING ORGANIZATION REPORT NUMBER

9. SPONSORING/MONITORING AGENCY NAME(S) AND ADDRESS(ES)
U.S. Army Research Office
P.O. Box 12211
Research Triangle Park, NC 27709-2211

10. SPONSOR/MONITOR'S ACRONYM(S)
ARO

11. SPONSOR/MONITOR'S REPORT NUMBER(S)
53027-MS-DRP.1

12. DISTRIBUTION AVAILIBILITY STATEMENT
Approved for Public Release; Distribution Unlimited

13. SUPPLEMENTARY NOTES
The views, opinions and/or findings contained in this report are those of the author(s) and should not contrued as an official Department of the Army position, policy or decision, unless so designated by other documentation.

14. ABSTRACT
The goal of the research was to demonstrate a revolutionary advancement in nanometer-scale imaging, using an array of atomic force microscope cantilever tips to image an area of unprecedented size. The key technical challenge in large are nanoimaging is to develop scalable cantilever arrays where each cantilever can be independently actuated and sensed.

15. SUBJECT TERMS
nanometrology, nanotechnology, scanning probe microscopy, materials analysis

| 16. SECURITY CLASSIFICATION OF: | | | 17. LIMITATION OF ABSTRACT | 15. NUMBER OF PAGES | 19a. NAME OF RESPONSIBLE PERSON |
|---|---|---|---|---|---|
| a. REPORT | b. ABSTRACT | c. THIS PAGE | | | William King |
| UU | UU | UU | UU | | 19b. TELEPHONE NUMBER 217-244-3864 |

**Report Title**

High Speed Imaging using Nanoprobe Arrays


**ABSTRACT**

The goal of the research was to demonstrate a revolutionary advancement in nanometer-scale imaging, using an array of atomic force microscope cantilever tips to image an area of unprecedented size. The key technical challenge in large are nanoimaging is to develop scalable cantilever arrays where each cantilever can be independently actuated and sensed.


## Enter List of papers submitted or published that acknowledge ARO support from the start of the project to the date of this printing. List the papers, including journal references, in the following categories:

### (a) Papers published in peer-reviewed journals (N/A for none)

Lee, J. and W. P. King, "Microcantilever Actuation via Periodic Internal Heating," Review of Scientific Instruments, 78, 126102, 2007. Republished online in the Virtual Journal of Nanoscience & Nanotechnology.

Received Paper

Lee, J. and W. P. King, "Improved All-Silicon Microcantilever Heaters with Integrated Piezoresistive Sensing," Journal of Microelectromechanical Systems, 17:2, April 2008.

**TOTAL:**

**Number of Papers published in peer-reviewed journals:** 2.00

### (b) Papers published in non-peer-reviewed journals (N/A for none)

Received Paper

**TOTAL:**

**Number of Papers published in non peer-reviewed journals:** 0.00

### (c) Presentations

Lee, J. and W. P. King, "Heated Atomic Force Microscope Cantilevers for Nanoscience and Nanoengineering," International Scanning Probe Microscopy Conference, Seattle, WA, July 2008.

**Number of Presentations:** 1.00

### Non Peer-Reviewed Conference Proceeding publications (other than abstracts):

Received Paper

**TOTAL:**

**Number of Non Peer-Reviewed Conference Proceeding publications (other than abstracts):** 0

## Peer-Reviewed Conference Proceeding publications (other than abstracts):

Received Paper

**TOTAL:**

**Number of Peer-Reviewed Conference Proceeding publications (other than abstracts):** 0

## (d) Manuscripts

Received Paper

**TOTAL:**

**Number of Manuscripts:** 0.00

## Books

Received Paper

**TOTAL:**

## Patents Submitted

## Patents Awarded

## Awards

### Graduate Students

| NAME | PERCENT_SUPPORTED |
|---|---|
| Jungchul Lee | 1.00 |
| **FTE Equivalent:** | **1.00** |
| **Total Number:** | **1** |

### Names of Post Doctorates

| NAME | PERCENT_SUPPORTED |
|---|---|
| **FTE Equivalent:** | |
| **Total Number:** | |

### Names of Faculty Supported

| NAME | PERCENT_SUPPORTED | National Academy Member |
|---|---|---|
| William P. King | 0.05 | No |
| **FTE Equivalent:** | **0.05** | |
| **Total Number:** | **1** | |

### Names of Under Graduate students supported

| NAME | PERCENT_SUPPORTED |
|---|---|
| **FTE Equivalent:** | |
| **Total Number:** | |

### Student Metrics

This section only applies to graduating undergraduates supported by this agreement in this reporting period

| | |
|---|---|
| The number of undergraduates funded by this agreement who graduated during this period: ..... | 0.00 |
| The number of undergraduates funded by this agreement who graduated during this period with a degree in science, mathematics, engineering, or technology fields:..... | 0.00 |
| The number of undergraduates funded by your agreement who graduated during this period and will continue to pursue a graduate or Ph.D. degree in science, mathematics, engineering, or technology fields:..... | 0.00 |
| Number of graduating undergraduates who achieved a 3.5 GPA to 4.0 (4.0 max scale): ..... | 0.00 |
| Number of graduating undergraduates funded by a DoD funded Center of Excellence grant for Education, Research and Engineering: ..... | 0.00 |
| The number of undergraduates funded by your agreement who graduated during this period and intend to work for the Department of Defense ..... | 0.00 |
| The number of undergraduates funded by your agreement who graduated during this period and will receive scholarships or fellowships for further studies in science, mathematics, engineering or technology fields: ..... | 0.00 |

## Names of Personnel receiving masters degrees

| NAME |
| --- |
| **Total Number:** |

## Names of personnel receiving PHDs

| NAME | |
| --- | --- |
| Jungchul Lee | |
| **Total Number:** | **1** |

## Names of other research staff

| NAME | PERCENT_SUPPORTED |
| --- | --- |
| **FTE Equivalent:** | |
| **Total Number:** | |

## Sub Contractors (DD882)

## Inventions (DD882)

## Scientific Progress

# Technology Transfer

**FINAL REPORT Agreement No. W911NF-07-1-0390**

# HIGH SPEED LARGE AREA NANOIMAGING USING PROBE ARRAYS

William King
Department of Mechanical Science and Engineering
University of Illinois Urbana-Champaign
1206 West Green St. Urbana, IL 61801
Phone: (217) 244-9956 | Fax: (217) 244-6534
Email: wpk@illinois.edu

## Statement of the problem studied

The goal of the research was to demonstrate a revolutionary advancement in nanometer-scale imaging, using an array of atomic force microscope cantilever tips to image an area of unprecedented size. The key technical challenge in large are nanoimaging is to develop scalable cantilever arrays where each cantilever can be independently actuated and sensed.

## Summary of the most important results

For this project we developed an array of atomic force microscope cantilevers that were then integrated into a commercial scanning probe microscope system and used to scan a surface. This represents the first time that a cantilever array was used in a commercial scanning probe system for parallel nanometrology. To the best of our knowledge, this is the first ever demonstration of parallel nanometrology with a cantilever array. Our approach for doing so is high scalable, and could be scaled to the meter scale with a sufficiently large microcantilever array. The cantilevers in our array can each be individually addressed for either contact mode scanning or "tapping" mode noncontact scanning. The ability to individually address the cantilevers is the key requirement for scaling the cantilever array. Two journal articles follow that resulted from this project, which contain many details of the technical results from this project.

## Bibliography

Lee, J., and W. P. King, "Improved All-Silicon Microcantilever Heaters with Integrated Piezoresistive Sensing," Journal of Microelectromechanical Systems, 17:2, April 2008.

Lee, J. and W. P. King, "Microcantilever Actuation via Periodic Internal Heating," Review of Scientific Instruments, 78, 126102, 2007.

# Topography imaging with a heated atomic force microscope cantilever in tapping mode

Keunhan Park, Jungchul Lee, and Zhuomin M. Zhang
*Woodruff School of Mechanical Engineering, Georgia Institute of Technology, Atlanta, Georgia 30332*

William P. King[a)]
*Department of Mechanical Science and Engineering, University of Illinois Urbana-Champaign, Urbana, Illinois 61801*

(Received 27 January 2007; accepted 12 March 2007; published online 30 April 2007)

This article describes tapping mode atomic force microscopy (AFM) using a heated AFM cantilever. The electrical and thermal responses of the cantilever were investigated while the cantilever oscillated in free space or was in intermittent contact with a surface. The cantilever oscillates at its mechanical resonant frequency, 70.36 kHz, which is much faster than its thermal time constant of 300 $\mu$s, and so the cantilever operates in thermal steady state. The thermal impedance between the cantilever heater and the sample was measured through the cantilever temperature signal. Topographical imaging was performed on silicon calibration gratings of height 20 and 100 nm. The obtained topography sensitivity is as high as 200 $\mu$V/nm and the resolution is as good as 0.5 nm/Hz$^{1/2}$, depending on the cantilever power. The cantilever heating power ranges 0–7 mW, which corresponds to a temperature range of 25–700 °C. The imaging was performed entirely using the cantilever thermal signal and no laser or other optics was required. As in conventional AFM, the tapping mode operation demonstrated here can suppress imaging artifacts and enable imaging of soft samples. © *2007 American Institute of Physics.* [DOI: 10.1063/1.2721422]

## I. INTRODUCTION

The atomic force microscope[1] (AFM) has emerged as perhaps the most widely used tool for sensing nanometer-scale surface features. In the most common AFM configuration, the features of a surface can be measured through the cantilever position, which is detected by a laser reflected from the cantilever. However, laser-deflection based AFM is not feasible in every situation, for example when large arrays of cantilevers are to be operated in parallel or when the system does not permit optical access. In these situations, alternative approaches to monitor the cantilever position are required.

One alternative to monitor the cantilever position is to measure heat flow from the probe. The first report of local probes that exploit heat flow to sense topography was performed with a profilometer tip affixed with a thermocouple.[2] The thermocouple temperature signal indicated the amount of heat flow between the tip and the surface, which was modulated by the distance between the tip and the sample. The thermal signal could thus be used as a feedback signal for measuring topography. The same sensing strategy was possible with silicon cantilevers that had solid-state heater-thermometers:[3] in the case of the silicon probe, the temperature sensor was a thermistor rather than a thermocouple. Silicon AFM cantilevers with integrated heaters were originally developed for data storage,[3–6] but have also been used for nanometer-scale thermophysical measurements[7–9] and manufacturing.[10–14] Recent theoretical[15,16] and experimental[17] studies showed that heated AFM cantilevers can be used for imaging nanometer-scale surface topography with sensitivity that greatly exceeds that of the piezoresistive cantilever. The thermally sensed topography was also suggested by Lee and Gianchandani[18] with a different type of scanning thermal probe. However, these previous studies have been strictly limited to contact-mode operation and no published report has described the use of the heated cantilever in tapping-mode operation. As in conventional tapping-mode AFM,[19–21] the use of a heated cantilever in tapping mode would allow precise topographic imaging of soft samples while suppressing imaging artifacts.

This article explores the resolution and sensitivity of heated AFM cantilevers used in tapping mode imaging. The cantilever electrical and thermal characteristics are monitored when the cantilever oscillates either in free space or in intermittent contact with a surface. The cantilever electrical signal is compared to the laser-deflection signal. Several important issues are highlighted regarding cantilever design and operation for tapping mode imaging.

## II. EXPERIMENT

The experiment used heated microcantilevers made from a silicon-on-insulator wafer.[4,22] Figure 1 shows the scanning electron microscope (SEM) image of the cantilever used in the experiment. The cantilever is u-shaped, having the heater integrated at the free end. The tip is fabricated at the center of the heater region with the height of around 500 nm and tip radius of 20–50 nm. The cantilever thickness is around 1 $\mu$m. The heater region is highly resistive region of 8 $\mu$m

[a)]Electronic mail: wpk@uiuc.edu

 

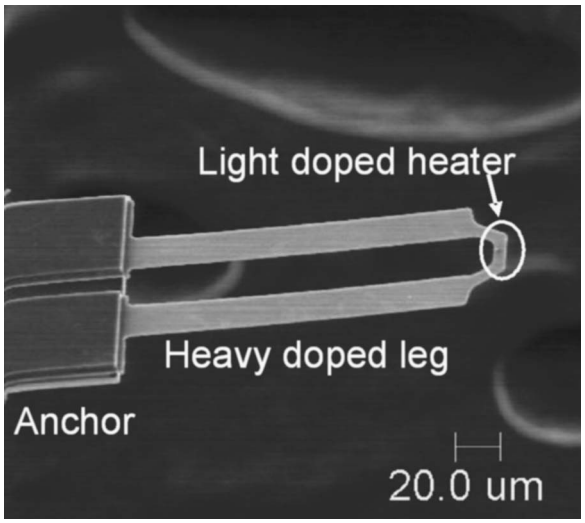


FIG. 1. SEM image of the cantilever with integrated heater used in the experiment. The cantilever is made of single crystal silicon, with high phosphorus doping in the leg region and low phosphorus doping in heater region.

$\times 16\ \mu$m that is realized with light phosphorus doping of around $10^{17}$ cm$^{-3}$. When the electrical current flows through the cantilever, the heater region dissipates more than 90% of the electrical power, resulting in temperature rise over 1000 K.[22] The leg region, whose length and width are, respectively, 150 and 15 $\mu$m, is heavily phosphorus doped to around $10^{20}$ cm$^{-3}$ for electrical leads. The anchor that connects the base silicon and the cantilever creates the buffer zone that mitigates any inconsistency of the backside etching process and allows for improved laser access when mounted on a commercial AFM system.

The concept of topography mapping using the cantilever thermal signal has been explained previously[17] and is briefly summarized here. When the heated cantilever is operated near a surface, most of the generated heat flows into the substrate. About half of the heat flows directly across the air gap, while the remainder flows into the cantilever legs, although most of the heat that flows into the legs eventually flows into the air and into the substrate. The heat flow from the cantilever is a strong function of the air gap[17]

$$k_{\text{eff}} = \frac{\bar{k}}{\lambda}\left(\frac{1}{\lambda} + \frac{C}{g}\right)^{-1}, \tag{1}$$

where $\bar{k}$ is the effective thermal conductivity of air bounded by parallel surfaces; $\lambda$ is the mean free path of air, which is approximately 70 nm; coefficient $C$ is on the order of 1 and can be estimated from rarefied gas dynamics for free molecule flow; and $g$ is the cantilever-substrate gap. Equation (1) shows that the heat transfer to the substrate is a function of the air gap. As the heated cantilever scans over a substrate, topographical feature of the substrate changes the vertical displacement of the cantilever relative to the substrate, leading to the change of the cantilever heater temperature and, correspondingly, the cantilever resistance. Thus, monitoring the cantilever voltage whle the heated cantilever scans the surface can provide the topographic image as the laser-deflection measurement does in tapping mode.

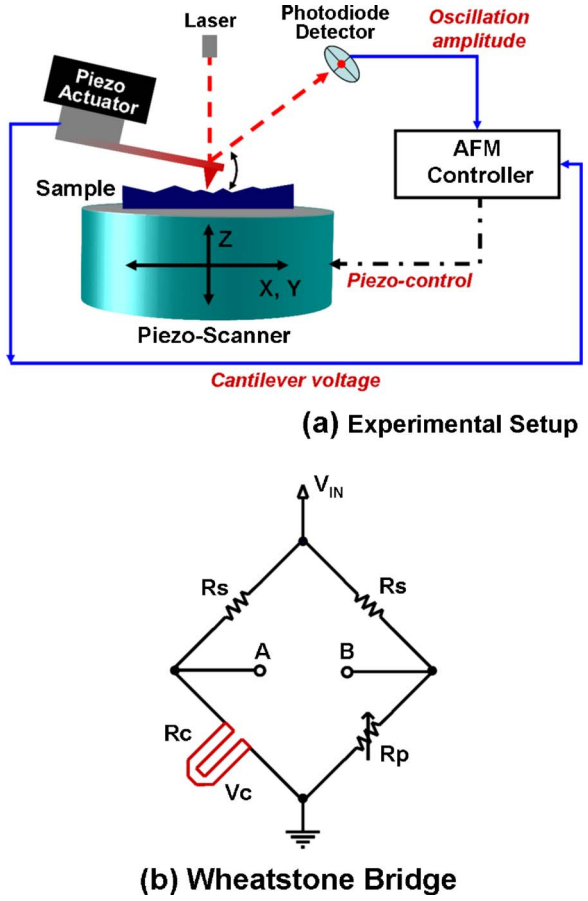


FIG. 2. (a) The experimental setup for tapping mode topographical imaging using a heated microcantilever. While oscillating the cantilever, the AFM controller measures the laser deflection using a position-sensitive PSD. The temperature-dependant voltage of the cantilever heater is measured simultaneously. (b) The use of Wheatstone bridge enhances the sensitivity of the cantilever voltage measurement. The cantilever voltage change can be obtained with $\Delta V_C = V_A - V_B$.

The experiment was performed in a commercial AFM platform (Asylum MFP-3D). Figure 2(a) illustrates the experimental setup of tapping mode topography using a heated microcantilever. While the cantilever scanned over a sample in tapping mode, the AFM controller provided a topographic image of the sample by modulating the oscillation amplitude of the cantilever measured with a position-sensitive photodiode detector (PSD).[19–21] At the same time, the cantilever was operated in a Wheatstone bridge circuit, as shown in Fig. 2(b). When the electrical current flows through the bridge circuit, the cantilever dissipates the electrical power and increases the heater temperature. Since the cantilever resistance is dependent upon the heater temperature, measuring the voltage change between $A$ and $B$, i.e., $\Delta V_C = V_A - V_B$, provides the relative change of the cantilever heater temperature. Measuring $\Delta V_C$ during the raster scanning can thus provide thermally sensed topography. In the experiment, 5 k$\Omega$ noninductive resistors were used for the Wheatstone bridge.

## III. RESULTS AND DISCUSSION

Before operating the cantilever in tapping mode, the cantilever mechanical properties of the cantilever must be understood. Figure 3 shows the thermal noise spectrum of the

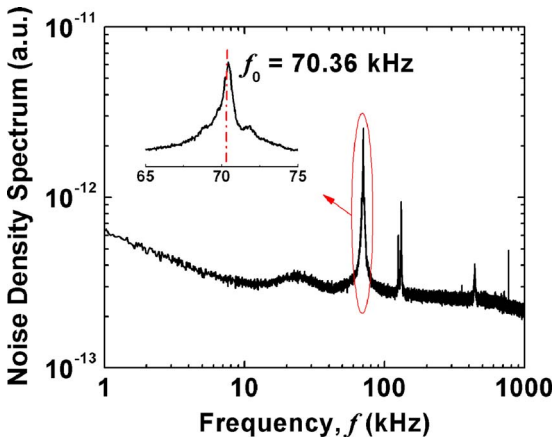


FIG. 3. The mechanical characteristics of the cantilever when it is suspended in quiescent air, without interacting with the substrate. The noise density spectrum of the cantilever provides the fundamental mechanical resonance frequency of the cantilever.

cantilever, which is the Fourier transformed laser-deflection signal of the unheated, free-standing cantilever far from the substrate. The random movement of air particles and their collisions to the cantilever give rise to the random fluctuation of the cantilever. As shown in the inset of Fig. 3, the fundamental resonance frequency can be obtained from the first peak position at 70.36 kHz. The other peaks at higher frequencies are due to higher oscillation modes or different oscillation patterns caused by the "U" shape of the cantilever. Another important property is the inverse optical lever sensitivity (InvOLS), which is a parameter that converts laser-deflection signal to the oscillation amplitude. The InvOLS can be obtained from a slope of laser-deflection signal against the change of the $z$-direction piezoscanner when the cantilever is in contact with the substrate. The InvOLS of the cantilever used in the experiment was 330 nm/V. The driving frequency for tapping mode was chosen as 69.5 kHz, close to the resonance frequency.

Electrical characterization of the cantilever is also necessary for the topography measurement. Figure 4(a) shows the cantilever resistance as a function of the total input voltage when the cantilever is suspended in quiescent air, without interacting with the substrate. The cantilever resistance first increases with increasing input voltage because of the decreasing electrical mobility of doped silicon with temperature. At 10 V input voltage, however, the cantilever resistance begins to decrease because the thermally generated intrinsic carriers outnumber the background doped carriers. This decreasing resistance is a characteristic of the thermal runaway behavior, which is typically observed in doped silicon devices.[23] To see any thermal effect on the cantilever due to its oscillation, the cantilever was characterized when it was in oscillation with the frequency of 69.5 kHz and compared with the characterization result when the cantilever was steady: the two cases are nearly identical. Figure 4(b) provides more details of the cantilever oscillation effect on the cantilever thermal behavior by showing the cantilever voltage spectrum measured with a spectrum analyzer. As shown in the inset of Fig. 4(b), there exists a peak in the cantilever voltage spectrum at the driving frequency, indicating that the cantilever voltage oscillates due to the mechanical oscillation of the cantilever. The peak value of 140 $\mu$V-rms at zero input voltage suggests that a part of the peak signal is attributed to the noise pickup from the dithering piezoactuator. As the input voltage increases, the peak value increases in a very similar manner to the direct current (dc) cantilever voltage in Fig. 3(a), implying that the cantilever is thermally affected by the cantilever oscillation. However, this thermal effect of the cantilever oscillation can be ignored because the peak value is negligibly small compared to the dc cantilever voltage.

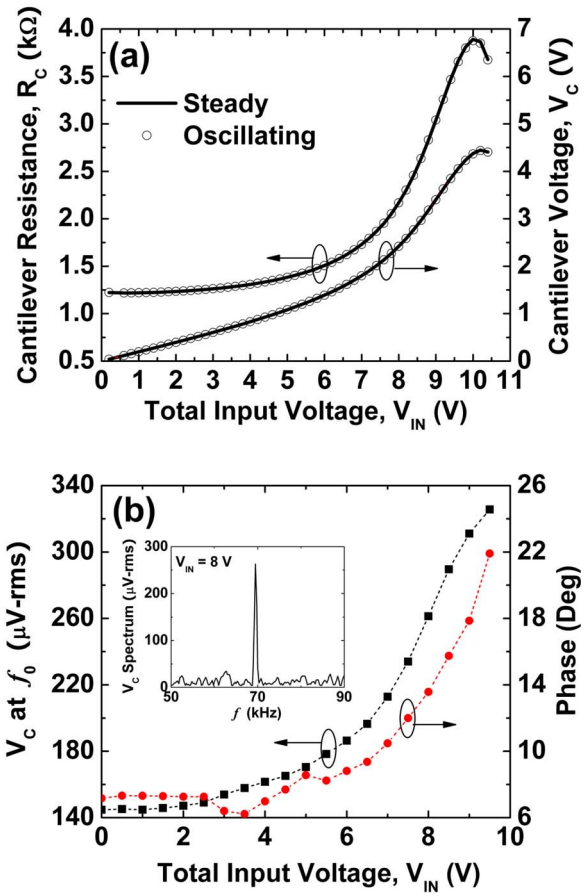


FIG. 4. The effect of mechanical oscillation of the cantilever on the cantilever thermal response. (a) The cantilever resistance curves as a function of the input voltage when it is suspended in steady and in oscillation. The cantilever resistance nonlinearly increases with the increase of the total input voltage. The dc cantilever thermal response is nearly the same for the case of cantilever oscillation held steady. (b) Due to the cantilever oscillation, the spectrum of the cantilever voltage shows a peak at the dithering frequency at 69.5 kHz. This peak is, however, less than 0.01% of the total cantilever voltage.

Such a negligible oscillation effect on the cantilever thermal behavior can be explained with two reasons. The first reason is due to the fast cantilever oscillation with small amplitude. During the measurement, the oscillation frequency was 69.5 kHz, and the oscillation amplitude was 1.5 V in laser-deflection signal, or 495 nm from the InvOLS. Even though the cantilever oscillation may agitate the surrounding air and thus change the heat transfer rate to the air, such small and fast oscillation will not have much effect on the cantilever behavior. The second reason is because the cantilever oscillates much faster than its thermal time con-

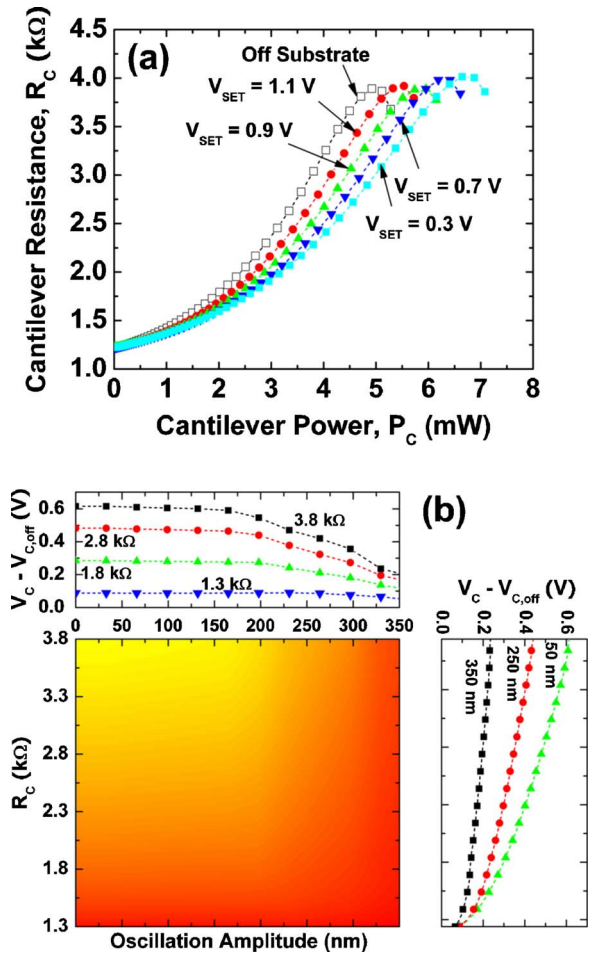


FIG. 5. The effect of the substrate when approaching the heated cantilever to a silicon substrate. (a) As the cantilever approaches the substrate, more heat is transferred from the cantilever to the substrate. Thus, the dc characteristic curves shifts to the higher cantilever power by the amount of increased heat flow rate to the substrate. (b) The contour of the cantilever voltage as a function of the cantilever resistance and cantilever oscillation amplitude. The cantilever is fully engaged to the substrate when the cantilever amplitude decreases below 150 nm. From that point, the cantilever voltage does not change with further decrease of the oscillation amplitude.

stant. Previous research clarified that the thermal time constant of a heated cantilever having the same geometry as the present work is in the order of 300 $\mu$s, which corresponds to 3.3 kHz in frequency.[24] This frequency is much lower than the oscillation frequency of the cantilever, suggesting that the cantilever does not have enough time to thermally respond to the disturbance resulting from the cantilever oscillation.

Electrical characterization was performed when the cantilever was engaged to the substrate with different set points, $V_{SET}$. When the cantilever is operated in tapping mode, the set point defines the oscillation amplitude of the cantilever: a larger set point provides larger oscillation amplitude. Figure 5(a) shows the cantilever resistance curves as a function of the power dissipation of the cantilever. When compared to the off-substrate operation, the resistance curve shifts to the large cantilever power as the set point decreases. This shift is because more heat is transferred to the substrate as the cantilever-substrate gap is reduced. Finally, when the set point becomes 0.3 V, the resistance curve does not shift any more as the cantilever tip overcomes the air-damping and touches the substrate: true engagement occurs. Figure 5(b) shows the cantilever voltage change relative to that of the off-substrate characterization in Fig. 5(a), for various cantilever resistances and oscillation amplitudes. It should be noted that the cantilever oscillation amplitude is obtained from the set point and InvOLS. From the horizontal profile in the top plot, it is clear that the cantilever voltage becomes saturated as the oscillation amplitude decreases below around 150 nm, or 0.4 V in set point. Thus, monitoring the cantilever voltage can provide the true engagement point without relying on the laser metrology. The vertical profile at the right plot shows the cantilever voltage as a function of the cantilever resistance for several fixed oscillation amplitudes. As expected, the cantilever voltage increases with increasing cantilever resistance, but the increasing pattern is not linear.

Once the heated cantilever is fully engaged to the substrate, the topographic image of the sample can be obtained by monitoring the $z$-direction piezoscanner that moves to maintain a tapping amplitude, and also by monitoring the cantilever voltage, $\Delta V_C$, that varies due to the relative change of the cantilever-substrate gap. It should be noted that even though the cantilever tip taps the substrate in oscillation, the cantilever is in thermally steady state, not sensing the oscillation, due to its large thermal time constant. Thus, regardless of the operation mode, simply measuring $\Delta V_C$ during raster scanning enables the topographic imaging. As a proof of concept demonstration, Figs. 6(a) and 6(b), respectively, show the laser-deflection based topographic image and the thermally sensed topographic image of the standard silicon gratings of 100 nm height. While in tapping mode with the set point of 0.3 V, the total input voltage was maintained with 9 V that corresponded to the cantilever resistance of 2.07 kΩ and the cantilever power of 3.35 mW. Qualitatively, the thermally sensed topographic image is almost the same as the laser-deflection based image except that the thermally sensed topographic image has a little bit bigger noise, which will be discussed in the following paragraph. Quantitatively, the cantilever voltage changes from -4 to 6 mV while the grating height changes from -40 to 60 nm, yielding the sensitivity of 100 $\mu$V/nm when the sensitivity is defined as[16]

$$S = \frac{|\Delta V_C|}{\Delta z}, \tag{2}$$

where $S$ is the sensitivity and $\Delta z$ is the vertical displacement of the cantilever tip. The estimated sensitivity of 100 $\mu$V/nm is at least one order of magnitude better than that of the piezoresistive cantilever.[15,25,26] Moreover, when compared to the thermal topographic imaging in contact mode,[17] Fig. 6(b) does not have artificial peaks at the edge of the gratings that were observed in contact mode images. Through the experiment, we believe that these artificial peaks in contact mode are because the other part of the cantilever besides the tip undesirably touches the grating edge due to the contact force and corresponding deformation of the cantilever and can be prevented in tapping mode operation.

Since the thermally sensed topography is based on the cantilever resistance change, the quality of topographic imaging depends on the temperature coefficient of resistance

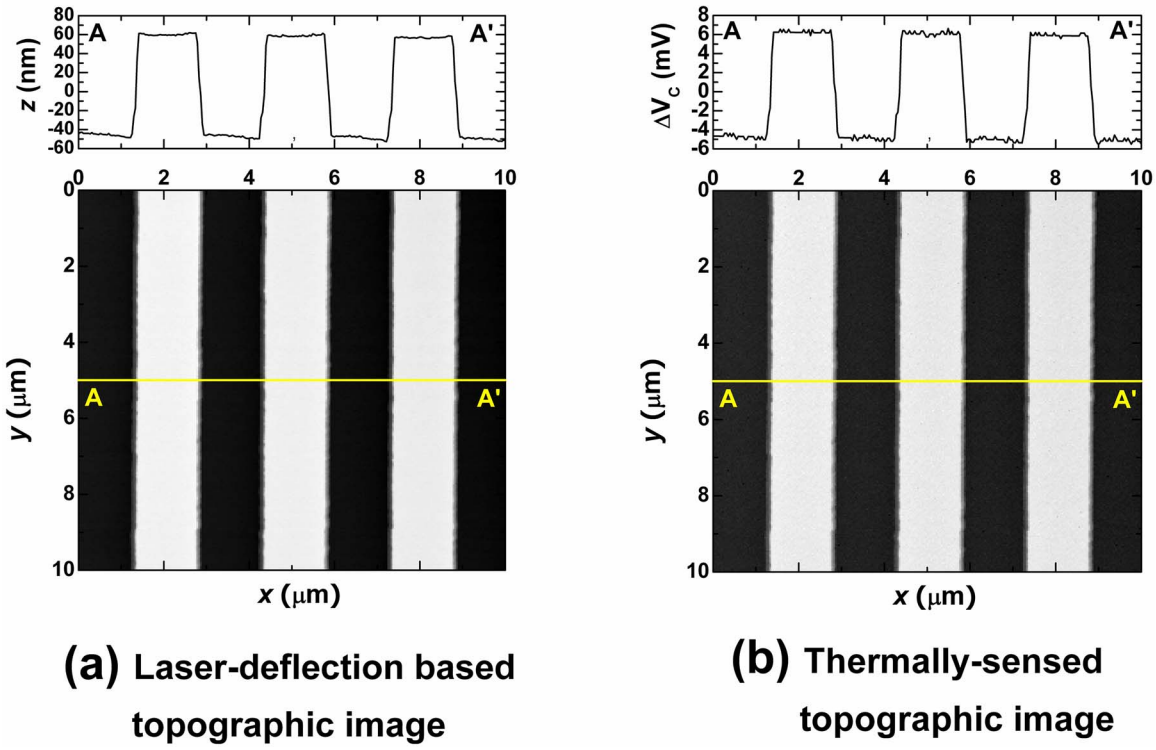


FIG. 6. (a) The laser-deflection based topography and (b) the thermally sensed topography of the 100 nm high Si gratings under the tapping mode. The total input voltage was 9 V. The thermally sensed topography was achieved by monitoring the cantilever voltage signal during scanning.

(TCR) of the cantilever. Figure 7(a) shows the cantilever resistance and qualitative change of topographical images for different input voltages when the set point is 0.3 V. It should be noted that only representative topographic images are shown in the figure although the experiment was performed at many input voltages. Apparently, the nonlinear TCR yields different images for the same gratings. At low power dissipation up to 2.5 mW (i.e., $V_{\mathrm{IN}}=8\mathrm{V}$), obtained images do not represent the true geometry as the TCR is not big enough for good topography. Good images can be obtained only when the slope is greater than $0.6\times10^{6}\ \Omega/\mathrm{W}$, which is shown with the line in Fig. 7(a). Thus, there exists an optimum cantilever operation range for a good thermal topography: for the heated cantilever used in the present study, the operation range is $4\ \mathrm{mW}<P_C<6.5\ \mathrm{mW}$ or $9.5\ \mathrm{V}<V_{\mathrm{IN}}<11.5\ \mathrm{V}$. If the cantilever is operated above the thermal runaway point, its negative resistance slope gives rise to the inversed topography.

For the evaluation of the thermally topographic imaging methodology, Fig. 7(b) shows the sensitivity and resolution obtained from topographic images of 100 and 20 nm tall gratings. As expressed in Eq. (2), the sensitivity is defined as the step change in cantilever voltage for 1 nm vertical displacement of the cantilever. The resolution means the smallest step change that could be measured in a given integration time, and thus can be calculated as the noise divided by the sensitivity.[16] In contact mode, the noise is the combination of thermal noise and Johnson noise under the assumption that there is no artifact in the signal.[15] However, the dominant noise in tapping mode comes from the peak at the tapping frequency, as shown in Fig. 4(b). To estimate the noise, the power spectral density of the peak at the tapping frequency was measured with a spectrum analyzer when the cantilever was engaged to the substrate. At lower input voltages, poor quality of topography is manifested with low sensitivity and bad resolution. As the input voltage increases, however, the sensitivity becomes better and finally saturated with around 200 $\mu\mathrm{V/nm}$ when the cantilever is operated above 10 V, which is consistent with the optimum operation range discussed earlier. This sensitivity curve shows a similar trend with the previous numerical study,[16] except the simulated sensitivity has a sharp dip where the cantilever resistance becomes maximal. Comparison with Fig. 7(a) suggests that there should be a dip between 11 and 12 V: it is technically not easy to observe the dip in experiment. The resolution also improves as the input voltage increases, realizing the subnanometer resolution. However, the overall resolution is one order of magnitude worse than the simulation results performed in contact mode,[16] as the peak noise at the tapping frequency is much larger than the thermally induced intrinsic noises.

The obtained experimental results reveal several important issues that should be considered when designing a heated cantilever as a tapping mode thermally-sensed topographic imaging tool. The first issue is the cantilever heater size. As mentioned earlier, the thermally-sensed topography can be realized by the heat transfer to the substrate and its sensitive change with the vertical displacement of the cantilever. Provided that over 90% of the cantilever power is dissipated in the heater,[22] the heater size has a dominant effect on the topographic imaging. If a feature size to be scanned is larger than the heater, the thermally-sensed topography will not be possible because the heater-substrate will not change. The cantilever tip height should be also carefully designed

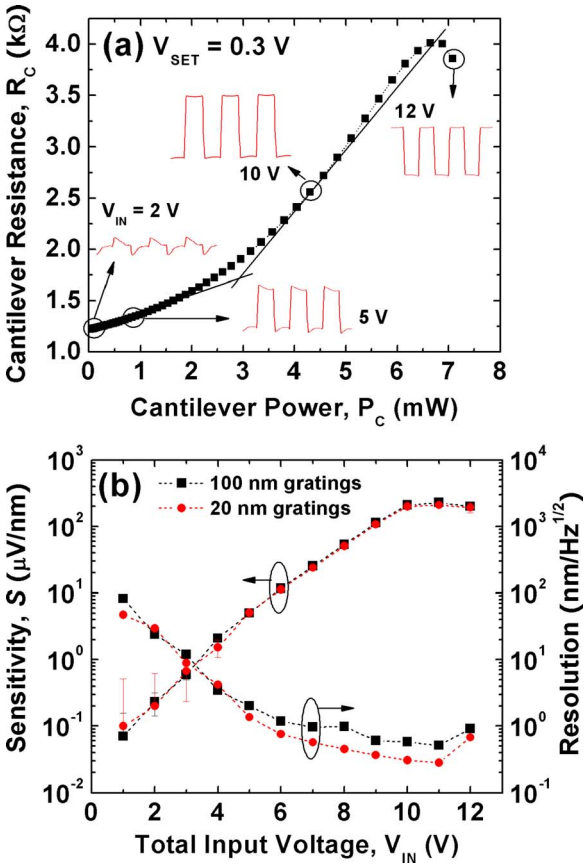


FIG. 7. The sensitivity and resolution of thermally sensed topography. (a) The cantilever resistance curve when the cantilever is engaged with the set point of 0.3 V. For lower cantilever power, the topographic image is distorted due to the poor sensitivity. Good images can be obtained at the high TCR region. When the cantilever is operated over the thermal runaway point, the topographic image is inversed due to the negative TCR. (b) The estimated sensitivity and resolution of the thermal topography metrology are obtained by scanning two Si gratings. The sensitivity can be as high as 200 $\mu$V/nm while the resolution is lower than 1 mm/$\sqrt{\text{Hz}}$.

and fabricated. If the tip is too high, the sensitivity would not be good.[16] However, if the cantilever tip height is too small, the cantilever-substrate heat transfer might enter the ballistic regime, in which the heat transfer rate is no more dependent upon the gap width:[27] topographic imaging could not be thermally obtained. The third issue to be considered is the thermal time constant of the cantilever. The successful thermally-sensed topography in the present study is attributed to the fact that the thermal time constant of the cantilever is larger than the inverse of the resonance frequency. Otherwise, the cantilever voltage would oscillate following the mechanical oscillation during scanning, complicating the accurate topography in tapping mode. The last issue is the doping level of the heater region. While the large input voltage enhances the sensitivity, it also drastically increases the heater temperature and may damage the sample that is vulnerable to heat. This undesirable heating can be prevented by lowering the doping level of the heater region, as the lower doping concentration yields higher resistance slope and thus enhances the sensitivity at lower temperature.[16] However, the resolution will become worse due to its high intrinsic noise. It should be noted that all the design parameters discussed here are strongly coupled together. Their crosstalk complicates the optimum design of the heated cantilever for a thermal topographic tool, and we suggest that this is an important future study.

## IV. SUMMARY

This work demonstrates thermally-sensed topographical imaging with a heated cantilever in tapping mode. The sensitivity is as high as 200 $\mu$V/nm and the resolution is as good as 0.5 nm/Hz$^{1/2}$, which are comparable to or better than other approaches. By characterizing the cantilever engaged to the substrate with different set points, we showed that the true engagement point can be thermally determined without the aid of the optics. Thus, the thermally-sensed AFM can be completely realized from the engagement to the topographic imaging. Since the thermally-sensed imaging technique eliminates the need for optical monitoring of the cantilever, the obtained results in the present study will enable the parallel displacement monitoring of cantilever arrays and even the development of portable AFM systems.

## ACKNLOWLEDGMENTS

This work was sponsored by the National Science Foundation (CTS-0327117, CAREER CTS-0338888), the Office of Naval Research, and DARPA.

[1] G. Binnig and C. F. Quate, Phys. Rev. Lett. **56**, 930 (1986).
[2] C. C. Williams and H. K. Wickramasinghe, Appl. Phys. Lett. **49**, 1587 (1986).
[3] G. Binnig *et al.*, Appl. Phys. Lett. **74**, 1329 (1999).
[4] B. W. Chui, T. D. Stowe, Y. S. Ju, K. E. Goodson, T. W. Kenny, H. J. Mamin, B. D. Terris, and R. P. Ried, J. Microelectromech. Syst. **7**, 69 (1998).
[5] W. P. King *et al.*, Appl. Phys. Lett. **78**, 1300 (2001).
[6] P. Vettiger *et al.*, IEEE Trans. NanoTechnol. **1**, 39 (2002).
[7] B. Gotsmann and U. Dürig, Langmuir **20**, 1495 (2004).
[8] B. Gotsmann and U. Dürig, Appl. Phys. Lett. **87**, 194102 (2005).
[9] W. P. King, S. Saxena, B. A. Nelson, R. Pitchimani, and B. L. Weeks, Nano Lett. **6**, 2145 (2006).
[10] P. E. Sheehan, L. J. Whitman, W. P. King, and A. N. Brent, Appl. Phys. Lett. **85**, 1589 (2004).
[11] B. A. Nelson, W. P. King, A. Laracuente, P. E. Sheehan, and L. J. Whitman, Appl. Phys. Lett. **88**, 033104 (2006).
[12] M. Yang, P. E. Sheehan, W. P. King, and L. J. Whitman, J. Am. Chem. Soc. **128**, 6774 (2006).
[13] B. Gotsmann, U. Dürig, J. Frommer, and C. J. Hawker, Adv. Funct. Mater. **16**, 1499 (2006).
[14] S. Bakbak, P. J. Leech, B. E. Carson, S. Saxena, W. P. King, and U. H. F. Bunz, Macromolecules **39**, 6793 (2006).
[15] W. P. King, T. W. Kenny, and K. E. Goodson, Appl. Phys. Lett. **85**, 2086 (2004).
[16] W. P. King, J. Micromech. Microeng. **15**, 2441 (2005).
[17] K. J. Kim, K. Park, J. Lee, Z. M. Zhang, and W. P. King, Sens. Actuators A available online (DOI 10.1016/j.sna.2006.10.052) (2007).
[18] J. H. Lee and Y. B. Gianchandani, Rev. Sci. Instrum. **75**, 1222 (2004).
[19] Y. Martin, C. C. Williams, and H. K. Wickramasinghe, J. Appl. Phys. **61**, 4723 (1987).
[20] Q. Zhong, D. Inniss, K. Kjoller, and V. B. Elings, Surf. Sci. **290**, L688 (1993).
[21] R. Garcia and R. Perez, Surf. Sci. Rep. **47**, 197 (2002).
[22] J. Lee, T. Beechem, T. L. Wright, B. A. Nelson, S. Graham, and W. P. King, J. Microelectromech. Syst. **15**, 1644 (2006).
[23] B. W. Chui, M. Asheghi, Y. S. Ju, K. E. Goodson, T. W. Kenny, and H. J. Mamin, Microscale Thermophys. Eng. **3**, 217 (1999).

[24] K. Park, J. Lee, Z. M. Zhang, and W. P. King, J. Microelectromech. Syst. available online (DOI 10.1109/jmems.2006.889498) (2007).
[25] T. Gotszalk, P. B. Grabiec, and I. W. Rangelow, Sens. Actuators, A **123–124**, 370 (2005).
[26] I. Shiraki, Y. Miyatake, T. Nagamura, and K. Miki, Rev. Sci. Instrum. **77**, 023705 (2006).
[27] J. B. Xu, K. Lauger, R. Moller, K. Dransfeld, and I. H. Wilson, J. Appl. Phys. **76**, 7209 (1994).

# Improved All-Silicon Microcantilever Heaters With Integrated Piezoresistive Sensing

Jungchul Lee and William P. King

***Abstract*—This paper presents the design, fabrication, and characterization of improved all-silicon microcantilever heaters with integrated piezoresistive sensing. The fabricated microcantilever heaters with piezoresistors are made solely from single crystal silicon with selective doping. Detailed characterization was performed to test the devices' electrical, thermal, and mechanical properties. The performance of and crosstalk between heater and piezoresistor elements were thoroughly tested. The resistive heater could reach temperatures of $> 600$ °C, and its temperature coefficient of electrical resistance was $(2.01 \pm 0.04) \times 10^{-3}$ $\Omega/\Omega \cdot$ °C. When biased at 2 V in a Wheatstone bridge, the deflection sensitivity of the piezoresistor was $(4.25 \pm 0.05) \times 10^{-4}$ V/V $\cdot \mu$m and remarkably, the heater circuit had a measurable deflection sensitivity of $(7.9 \pm 0.5) \times 10^{-5}$ V/V $\cdot \mu$m. Both the piezoresistor and the resistive heater were interfaced with a commercial atomic force microscope system to measure their sensitivities during topography imaging. The sensitivity of the thermal reading was much greater than that of piezoresistive reading. Noise-limited resolution of thermal reading was better than $0.46 \pm 0.03$ nm$/\sqrt{\text{Hz}}$ and piezoresistive reading was better than $3.4 \pm 0.4$ nm$/\sqrt{\text{Hz}}$. This is the first experimental comparison between thermal and piezoresistive topographic sensing, both of which can replace optical lever sensing. Four cantilevers in an array demonstrated parallel topographic sensing with both the heater and the piezoresistor. [2007-0107]**

***Index Terms*—Atomic force microscopy, cantilever array, crosstalk, heated cantilever, heating, microelectromechanical devices, micromachining, piezoresistive reading, piezoresistor, strain, temperature, thermal reading.**

## I. Introduction

MICROCANTILEVERS have shown versatility in various applications ranging from scanning probe microscopy (SPM) to bio/chemical sensing. Single microcantilevers are capable of subnanometer topographic resolution in SPM [1] and femtogram adsorption/desorption detection in bio/chemical sensing [2]. A common requirement in microcantilever applications is array parallelization to increase throughput or to test many analytes simultaneously. Array operation may also offer differential measurements that could cancel unwanted measurement artifacts.

Manuscript received May 13, 2007; revised January 6, 2008. Subject Editor C.-J. Kim.

The authors are with the Department of Mechanical Science and Engineering, University of Illinois at Urbana–Champaign, Urbana, IL 61801 USA (e-mail: wpk@uiuc.edu).

Color versions of one or more of the figures in this paper are available online at http://ieeexplore.ieee.org.

Digital Object Identifier 10.1109/JMEMS.2008.918423

Microcantilever probe arrays have been used in data storage [3]–[7], nanolithography [8], [9], parallel imaging [10], and force spectroscopy in life science applications [11]. Arrays having up to 64 × 64 microcantilevers with integrated heaters have been used to demonstrate probe-based data storage [12]. Each cantilever enabled writing, reading, and erasing of nanoscale indents on soft polymeric media [13]. A 100 × 100 array of thermopiezoelectric microcantilevers has been reported with further improved data bit density [14]. A multifunctional microcantilever probe array has been developed for nanoscale patterning and imaging using dip-pen nanolithography (DPN) and scanning probe contact printing [9]. A 2-D array having 55 000 cantilevers in 1 cm$^2$ was fabricated to achieve extremely large area DPN [15]. This is the highest density and largest number of cantilevers ever reported. A 4 × 4 array of piezoresistive microcantilever probes was specifically designed and fabricated to image biological cells in a buffer solution and to perform force spectroscopy measurements on cells [11].

Another application of microcantilever arrays is bio/chemical sensing where physisorption or chemisorption processes are transduced into mechanical responses [16]. In contrast to microcantilever probe arrays for imaging, these microcantilever arrays often operate far away from any substrate and do not require a tip. A 1 × 8 array of microcantilevers with selective coatings has been applied as an artificial nose to recognize and characterize alcohol vapors either in a static mode [17] or in a dynamic mode [18]. Besides, gas sensing, the same platform was introduced to investigate deoxyribonucleic acid (DNA) hybridization [16], antibody-antigen interaction [19], [20], and two different DNA-binding proteins [21]. Recently, a 2-D multiplexed array having 480 SiN/Au microcantilevers was fabricated to detect thermally induced phase transitions and stability of DNA [22].

Without regard to application, a major issue for the cantilever array operation is deflection sensing of each individual cantilever. For small arrays, optical sensing such as vertical-cavity surface-emitting lasers can be used [17], [18], [21]. However, having a large number of microcantilevers in the array requires integrated deflection sensing schemes, such as piezoelectric sensing [14], piezoresistive sensing [23], and capacitive sensing [24]. Among them, piezoresistive sensing has been widely used mainly because of the high sensitivity and ease of fabrication and implementation. Piezoresistive sensing has been shown to be very sensitive with subnanometer minimum detectable deflection [25] and can be used in both static and dynamic modes for bio/chemical sensing.

A thermal element fabricated into the cantilever permits detection of topographical features in data storage [26]. The

thermal detection mechanism has been thoroughly investigated in theoretical studies [27]–[29] and has been used for quantitative detection of nanometer-scale displacements [30] and for quantitative mapping of nanotopographical features [31], [32]. It has been suggested that the thermal sensing mechanism has a sensitivity that far exceeds that of piezoresistive sensing [27], [31]. However, no paper has made a direct comparison of the thermal and piezoresistive sensing mechanisms. The most compelling experiment that could be made would be using a cantilever having both piezoresistor and thermal elements. Microcantilevers having both a resistive microheater and a piezoresistor have been fabricated for data storage [3], [33] as well as calorimetry and mass detection [34]. These previous publications focused on cantilever fabrication and operation, but did not focus on detailed characterization of the cantilever heater and piezoresistor elements. From these papers, it is not possible to support or refute claims about the relative sensitivity of thermal versus piezoresistive sensing. The lack of a comprehensive characterization limits the development of similar cantilevers.

Microcantilevers having both heaters and piezoresistive sensors would be useful in a number of applications. One example is thermal nanomanufacturing [35], [36] where the tip heating would perform writing, but piezoresistive topography sensing would be preferred in the presence of a thermally reactive substrate. A second example is topography sensing where cantilever heating could be used to perform local materials synthesis [37], chemical reaction [38], or to clean the tip [39], [40]. Finally, such a cantilever could be used to sense temperature-sensitive biochemical binding events [22], [41].

This paper describes the design, fabrication, and characterization of a small array of microcantilever heaters with integrated piezoresistors. The heater and piezoresistor devices are thoroughly characterized during individual and simultaneous operation. This paper aims to thoroughly understand the links between cantilever design, fabrication, and performance, and to measure the relative performance of the heater and piezoresistive elements.

## II. Design, Simulation, and Fabrication

### A. Microcantilever Array Design

The design of the cantilever array is based on the silicon microcantilever heater reported in [42]. Fig. 1 shows the cantilever design, in which each cantilever has four legs. The two outer legs are highly doped to act as electrical leads to the resistive heater near the cantilever free end and the two inner legs will be used to define piezoresistors. Previous microcantilevers having both resistive heaters and piezoresistive sensors [3], [33] employed metal traces for carrying current. These metal traces placed limits on the device performance, including thermomechanical bending, temperature limits, and electromigration when the leads carried high current density. Here, we use doped silicon for the current-carrying traces as well as for the active heater and piezoresistive elements. By placing metal to doped silicon contacts far away from the hot spot, temperature at contacts can be greatly reduced. For a given current density

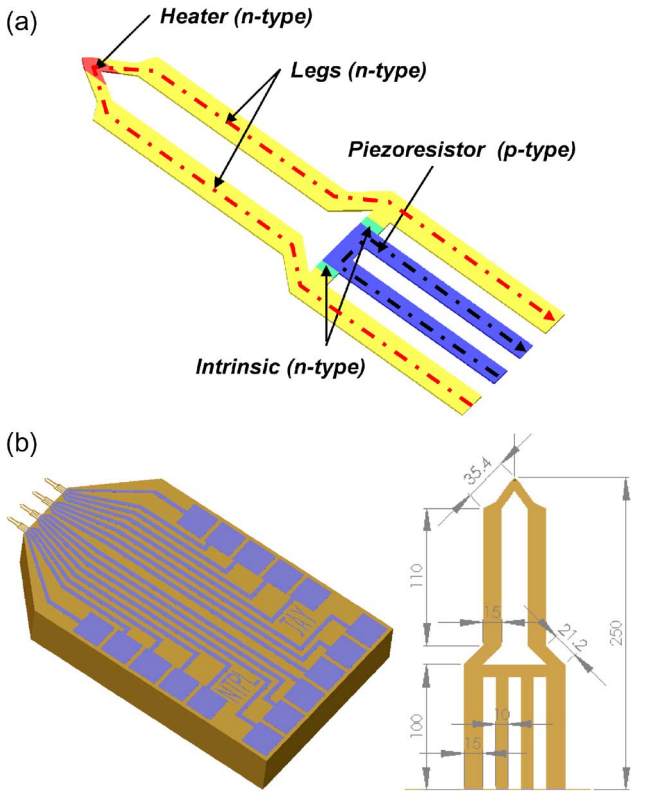


Fig. 1. (a) Single cantilever showing different doping regions for the heater, legs, and the piezoresistor. (b) Design of $1 \times 4$ array of microcantilever heaters with integrated piezoresistors and dimensions for an individual cantilever in micrometers.

$(J)$, when temperature $(T)$ at silicon to aluminum contacts is lowered from 400 K to 300 K, mean time to failure (MTF) given by [43]

$$\text{MTF} \propto \frac{1}{J^2} \exp\left(\frac{E_\text{A}}{k_\text{B}T}\right) \tag{1}$$

can be improved by about a factor of 3300 where $E_\text{A}$ is the activation energy of 0.84 eV for well-ordered and large-grained aluminum films [43] and $k_\text{B}$ is the Boltzmann constant. There are additional advantages using doped silicon current traces over metal traces on cantilevers. Since the melting point of silicon is much higher than that of frequently used metal as interconnects—for example, melting points of silicon and aluminum are 1412 °C and 660 °C, respectively—the temperature range for device operation can be significantly extended beyond 1000 °C. Therefore, higher current density can be accommodated at temperatures higher than the melting point of the metal without electromigration failure. While the packaged cantilever would not be able to operate in environments where the temperature exceeded the limits of the package or the metal–semiconductor junction, the local maximum temperature in the cantilever heater can far exceed these limits. By moving the metal–semiconductor junction away from the cantilever heater, the cantilever heater can reach higher temperatures than in some previous designs. Moreover, metals have a far different coefficient of thermal expansion (CTE) than silicon. It would be better not to use metals on cantilevers unless vertical bimorph actuation is required. For cantilevers using high-doped silicon

as current traces, no observable thermomechanical bending has been reported since CTE of the doped silicon layer is similar to that of intrinsic silicon. However, thermal bimorph bending $(d)$ of cantilevers with metal current traces given by [44]

$$d = \frac{3E_1E_2t_1t_2(t_1+t_2)l^2(\alpha_1-\alpha_2)\Delta T}{(E_1t_1^2)^2+(E_2t_2^2)^2+2E_1E_2t_1t_2\,(2t_1^2+3t_1t_2+2t_2^2)} \tag{2}$$

could range from a few micrometers to several tens of micrometers for typical cantilever dimension and temperature range of our interest, where $t$ is layer thickness, $l$ is cantilever length, $E$ is elastic modulus, $\alpha$ is CTE, $\Delta T$ is temperature change, and subscripts 1 and 2 denote metal current trace and silicon device layer.

The U-shaped cantilever is used to achieve thermal isolation between the heater and the piezoresistor. In addition, U-shaped design cantilevers have shown better performance in piezoresistive sensing than rectangular ones [45]. The length of the inner legs, which is equivalent to that of the piezoresistor, is chosen to be about 0.4 of the overall cantilever length, which is a design criterion that optimizes both resolution and sensitivity [46]. The clamped base is the preferred site for the piezoresistors to maximize deflection sensitivity. Fig. 1 shows the design of the microcantilever, the different dopant species and regions for the heater and the piezoresistor, and dimensions for an individual cantilever. To dope the active silicon elements, phosphorus was chosen for the heater and the two outer legs because phosphorus has a lower resistivity than boron at a given doping concentration [47]. However, boron was chosen for the piezoresistor to construct p-n junctions between the inner and the outer legs thus preventing electrical crosstalk between the heater and the piezoresistor. Similar approaches to minimize crosstalk have been reported using p-n junctions in two different directional piezoresistive elements [48] and Schottky diodes between each cantilevers in a cantilever array [5], [7]. In addition, boron has a higher piezoresistive coefficient than phosphorus in the $\langle 110\rangle$ crystal direction.

### *B. Mechanical and Electrical Simulation*

Because of the complex cantilever geometry, finite element simulation was required to obtain resonance frequency and spring constant. The finite element simulations allowed us to find appropriate analytical expressions of cantilever mechanical properties, which in turn allowed detailed design. To this end, static and eigenfrequency analyses in FEMLAB 3.1 (a finite element package, COMSOL, Inc.) were employed. Due to the complex cantilever geometry, the simulated resonance frequency and spring constant were not directly proportional to the cantilever thickness $(t)$ and its third power, respectively. However, plane view dimensions such as width and length are fixed; simulated resonance frequency $(f_0)$ and spring constant $(k)$ can be fitted with appropriate polynomials of cantilever thickness.

$$f_0(t)\ [\text{kHz}] = 0.534 + 25.688t \tag{3}$$

$$k(t)\ [\text{N/m}] = -3.306 + 3.299t - 1.088t^2 + 0.204t^3 \tag{4}$$

where thickness unit is micrometers and thickness ranges from 0.5 to 3.5 $\mu$m. The cantilever thickness can thus be easily estimated from (3) or (4) once either the resonance frequency or the spring constant is measured. To relate resonance frequency with spring constant, the microcantilever structure can be modeled as a simple harmonic oscillator, although the cantilever mass should be corrected. This corrected mass is often referred to as effective mass $(m_{\text{eff}})$. The resonance frequency of the microcantilever is

$$f_0 = \frac{1}{2\pi}\sqrt{\frac{k}{m_{\text{eff}}}} = \frac{1}{2\pi}\sqrt{\frac{k}{C_{\text{m}}m}} \tag{5}$$

where $m$ is the cantilever mass and $C_{\text{m}}$ is the correction factor. For example, the effective mass of a simple rectangular cantilever is 24% of the total mass. For the present cantilever, finite element simulations provide a correction factor of 0.148. These mechanical modeling facilitates cantilever calibration.

The microcantilever arrays are made of doped single crystalline silicon. To design doped silicon devices, it is important to estimate the resistivity and device resistance after implantation and diffusion since thermophysical properties and heating characteristics of doped silicon devices strongly depend upon local resistivity. Furthermore, the performance of a piezoresistor depends upon both doping concentration and the distribution of dopants in the silicon layer [46], [49]. To introduce dopants into the device layer in the microcantilever array, ion implantation was chosen over diffusion since implantation is a low-temperature process and offers more precise doping control. Since single crystalline silicon is the starting material, the introduction of a 7° wafer tilt angle during implantation prevents ion channeling such that the Gaussian distribution well describes doping profiles after implantation.

The implant energy, dose, and subsequent diffusion time were selected using a 1-D dopant diffusion simulator. The developed simulator incorporates both intrinsic and extrinsic diffusion to solve a diffusion equation described by Fick's first and second laws numerically. When the doping concentration is less than the intrinsic carrier concentration at diffusion temperature, diffusivity is independent of local doping concentration (intrinsic diffusion). However, diffusivity becomes concentration-dependent when the doping concentration exceeds the intrinsic carrier concentration (extrinsic diffusion). After local doping concentration was obtained from the diffusion simulation, the local electrical resistivity was calculated by $\rho = 1/[q(\mu_n N + \mu_p P)]$ where $q$ is the electron charge and $\mu_n$ and $\mu_p$ are electron and hole mobility, respectively. Bulk mobility models for electron and hole were adopted from [50]. Finally, calculated local resistivity was used to calculate device resistance per unit length using a parallel resistor network [51] and the actual device resistance was obtained considering the finalized geometry of the device. A commercial dopant diffusion simulator (SUPREME3) was used to check the results, and there was very close agreement between our simulation and the predictions of the commercial software. Fig. 2 shows predicted doping concentration and resistivity of low-doped phosphorus, high-doped phosphorus, and medium-doped boron that are obtained from the developed simulation.

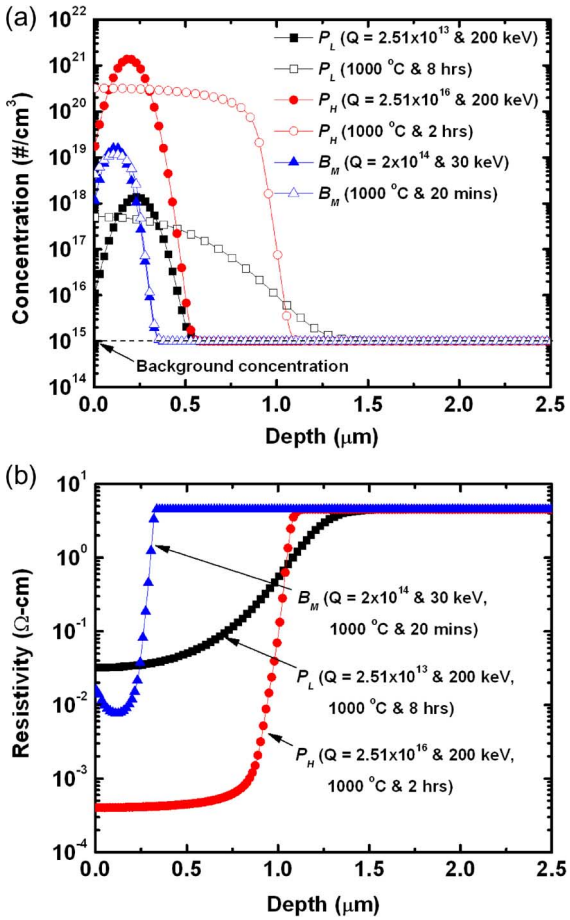


Fig. 2. (a) Simulated doping concentration of low-doped phosphorus, high-doped phosphorus, and medium-doped boron after implantation and postdiffusion. (b) Resistivity after implantation and postdiffusion. $P$ and $B$ indicate phosphorus and boron, respectively, and subscripts $H$, $M$, and $L$ denote high, intermediate, and low doping, respectively.

Simulated device resistances are compared with measurements in a following section.

### C. Microcantilever Array Fabrication

Fig. 3 shows the seven major fabrication steps to make the microcantilever array. The fabrication process starts with an $n$-type silicon-on-insulator wafer of orientation $\langle 100 \rangle$, where the silicon device layer is 5 $\mu$m, the buried oxide layer is 1 $\mu$m, and the silicon handle layer is 500 $\mu$m. Background doping in the device layer is $1 \times 10^{15}$ cm$^{-3}$ with a resistivity of approximately 4 $\Omega \cdot$ cm. The first step was to define a probe tip via dry isotropic silicon etch followed by oxidation sharpening. Then, photolithography patterned negative photoresist (Futurrex NR7-1500) to define the cantilever structures. A Bosch process using inductively coupled plasma (ICP) etched the patterned window all the way through the device layer until the buried oxide layer was fully exposed. After the probe tip and beam structures were defined in the device layer, three implantation steps were performed with hard-baked positive photoresist (Shipley 1827) as a mask for ion implantation. The first implantation doped the heater region near the free end with $2.51 \times 10^{13}$ cm$^{-2}$ of phosphorous at 200 keV. A postdiffusion step was performed for 6 h at 1000 °C in the furnace to distribute the implanted dopant uniformly. The second implantation step doped the two outer legs with $2.51 \times 10^{16}$ cm$^{-2}$ of phosphorous at 200 keV and a postdiffusion step was performed for 2 h at 1000 °C in the furnace. The two implantations finalized the $n$-type resistive heater. The final implantation defined the piezoresistor in the two inner legs with $2 \times 10^{14}$ cm$^{-2}$ of boron at 30 keV. The implanted boron was annealed for 20 min at 1000 °C in a rapid thermal processing chamber. After metallization and lift-off to define aluminum-doped silicon contacts, the backside of the handle wafer was etched using ICP until the buried oxide layer was exposed. The cantilever arrays were finally released by a 30 s dip in 49% hydrofluoric acid.

Arrays were batch-fabricated with 90% yield so that 200 fully functional arrays were extracted from a 100-mm wafer. Fig. 4(a) and (b) shows scanning electron micrographs (SEMs) of the fabricated microcantilever array. The inset in Fig. 4(a) shows the probe tip near the low-doped resistive heater. Fig. 4(c) shows a custom printed circuit board (PCB) to mount the array chip and a flexible ribbon cable for the electrical connection to the power supply and front end of data acquisition.

## III. Characterization

### A. Single Cantilever Characterization

After the array fabrication, individual microcantilever characterization was performed following the characterization techniques described in [42]. For the electrical testing, the cantilever was configured in series with precision 1 and 10 $k\Omega$ power resistors for the heater and piezoresistor, respectively. The cantilever was excited with dc voltage to investigate steady state responses. Fig. 5(a) shows the dc response of the heater defined near the free end and connected through the two outer highly conductive legs, which is typical of heated cantilevers [5], [42], [52], [53]. The critical power, $P_{\rm crit}$, at which the temperature coefficient of resistance (TCR) changes from positive to negative was 18 mW and the corresponding critical temperature, $T_{\rm crit}$, was 560 °C. The TCR changes signs due to thermal runaway in the doped silicon, which is well understood for microcantilever heaters [42]. Fig. 5(b) shows the dc response of the p-type piezoresistor defined in the two inner legs. Temperature data were collected using Raman spectroscopy as explained in detail in [42], [54], and [55]. Fig. 5(c) and (d) shows the comparison of the normalized electrical resistances of the heater and the piezoresistor as functions of power dissipation and maximum temperature in each doped resistor, respectively. From Fig. 5(d), the TCR of the doped resistor was obtained. The TCR of the heater was $(2.01 \pm 0.04) \times 10^{-3}$ $\Omega/\Omega \cdot$ °C and the TCR of the piezoresistor was $(8.3 \pm 0.4) \times 10^{-4}$ $\Omega/\Omega \cdot$ °C. The higher TCR in the heater is mainly due to its lower doping level, but also due to the different dopant type.

To test electrical crosstalk between the heater and the piezoresistor, two legs on the left or right were connected to a dc power (see inset in Fig. 6), and diode characteristics of the p-n junction were measured. Fig. 6 shows measured $I$–$V$ characteristics of the p-n junction between one leg for the

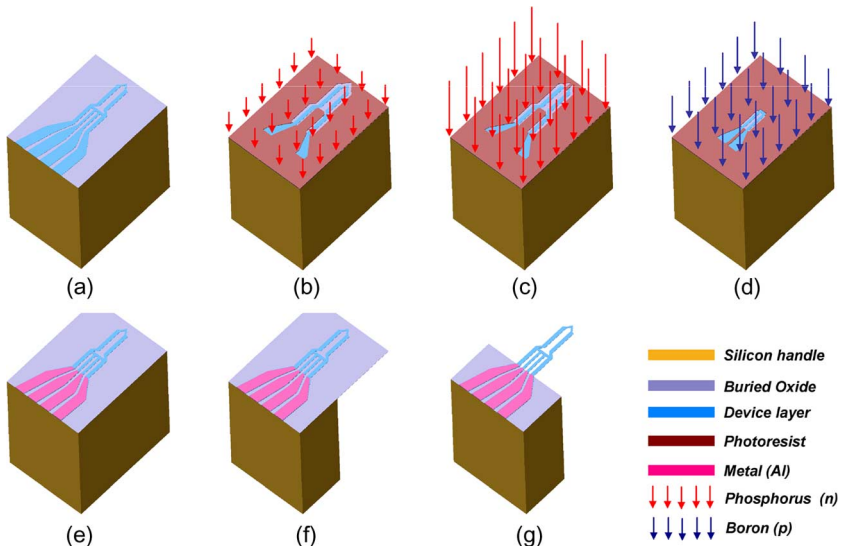


Fig. 3. Seven major fabrication steps to make the microcantilever heater array. (a) Tip/Beam. (b) Low dose implantation for heater/diffusion. (c) High dose implantation for heater legs/diffusion. (d) Intermediate dose implanatation for piezoresistors anneal (RTP). (e) Contact/Metallization. (f) Backside thru wafer etch. (g) Final device release.

heater and one leg for the piezoresistor for both forward and reverse bias. The on voltage (forward voltage drop) around 0.6 V is appropriate for a silicon p-n junction diode [56]. The breakdown voltage is around −10.5 V. However, there also exist Schottky barrier diodes and contact resistances between metal and doped silicon so that the measured $I$–$V$ characteristics cannot be simply expressed with an equivalent circuit of a p-n junction diode. When it is inevitable to have a voltage potential between two adjacent legs making a p-n junction (cross voltage potential), the bias direction needs to be determined carefully to minimize electrical crosstalk. Possible current leakages depend on the bias direction with the same cross voltage potentials. For example, the current flow could be only 3 $\mu$A for reverse bias or as high as 0.698 mA for forward bias with 3 V cross potential.

To test thermal crosstalk and to visualize the temperature field in the cantilever, the temperature distribution both in the heater and in the piezoresistor was investigated using IR microscopy (Infrascope II, Quantum Focus Instruments). Prior to temperature measurements, local emmissivity for each pixel was obtained from reference radiance calibration. Then, 50 measurements were made at about 1 Hz and averaged. A more detailed description of the experimental procedure can be found in [57]. Fig. 7 shows temperature distributions when the heater and the piezoresistor were heated to 5 mW, either individually or simultaneously. The apparent asymmetric temperature distribution and hot spot offsetting from the free end are due to intrinsic artifacts and spatial resolution limits in the IR setup. The Raman measurements provided accurate local temperature measurements. The additional 5 mW in the piezoresistor elevates the average temperature in the conductive legs but does not affect the maximum heater temperature since the heat generated in the piezoresistor is mostly dissipated into the adjacent air and the silicon handle. Only a small portion of this heat is directed to the free end of the cantilever. Despite the average temperature rise in the conductive legs, piezoresistive heating

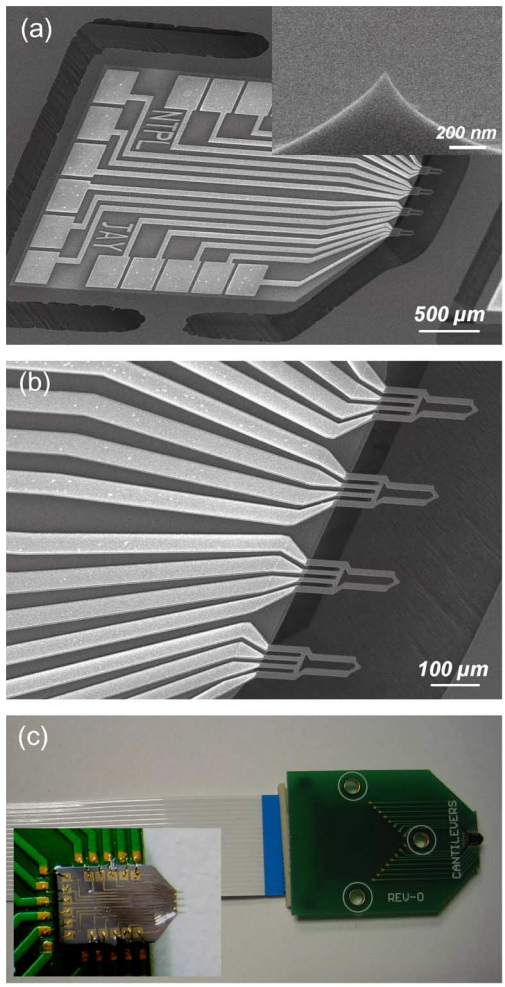


Fig. 4. (a) and (b) SEM images of the fabricated array chip. Inset in (a) shows the sharp tip near the low-doped resistive heater. (c) Custom PCB and flexible ribbon cable to mount an array chip and make electrical connections. Inset shows a wire-bonded array chip.

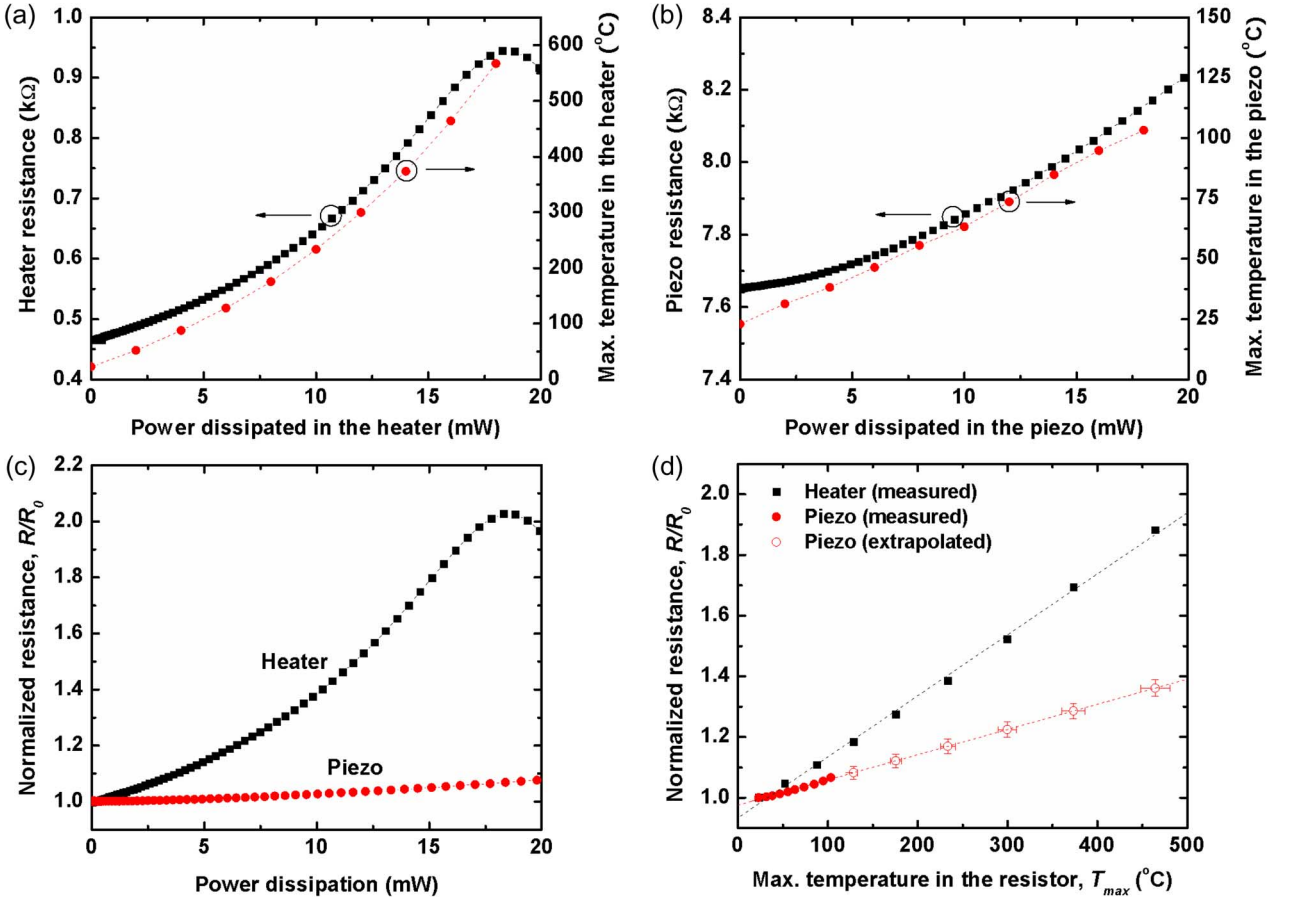


Fig. 5. (a) Electrical resistance and temperature of the heater as a function of power dissipation in the heater. (b) Electrical resistance and maximum temperature of the piezoresistor as a function of power dissipation in the piezoresistor. (c) Normalized resistance comparison between the heater and the piezoresistor. (d) Normalized resistance of the heater and the piezoresistor as a function of the maximum temperature in each resistor. Temperature data were obtained using Raman spectroscopy. These measurements are made on a free-standing cantilever far away from a substrate.

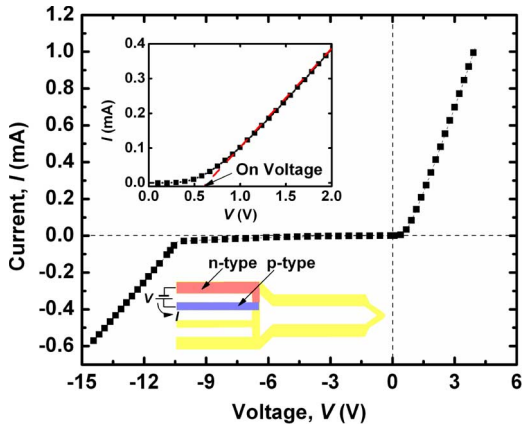


Fig. 6. $I$–$V$ characteristics of the p-n junction diode between one leg for the heater and one leg for the piezoresistor. The "on voltage" is around 0.6 V which is appropriate for silicon p-n diodes.

effect is negligible considering its contribution to the overall heater resistance and much lower TCR than the resistive heater. For practical uses, the power dissipation in the piezoresistor will be less than 1 mW so that the heater temperature can be maintained regardless of the piezoresistor operation. However, temperature rise in the piezoresistor due to the heater operation

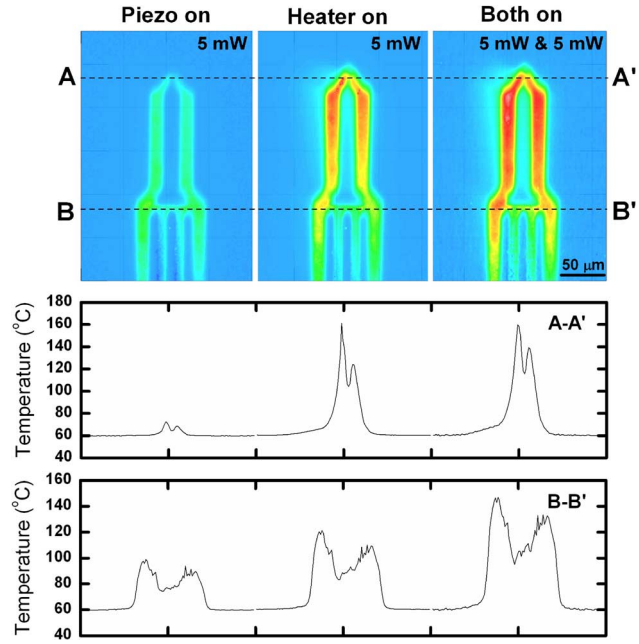


Fig. 7. IR micrographs with 5-mW power dissipation in the piezoresistor, 5-mW power dissipation in the heater, and 5-mW power dissipation in both the piezoresistor and the heater.

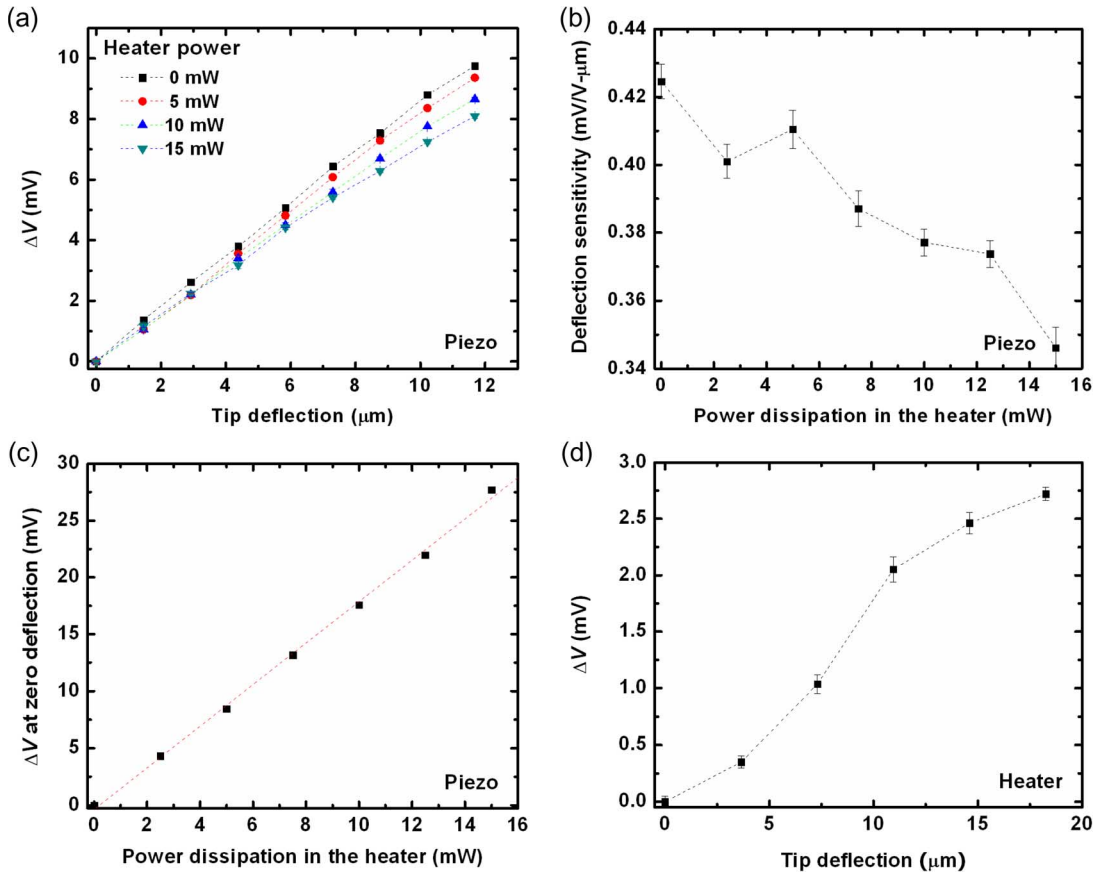


Fig. 8. Cantilever deflection sensitivity. (a) Bridge voltage output as a function of the tip deflection where bias voltage to the Wheatstone bridge is 2 V. Measurements are repeated with the heater powered. (b) Deflection sensitivity of the piezoresistors decreases as power dissipation in the heater increases. (c) Voltage offset linearly increases with power dissipation in the heater. (d) Voltage output from another bridge as a function of the tip deflection where bias voltage to the Wheatstone bridge is 2 V.

might not be negligible since high temperature heater operation is often required. For such cases, switching operation between two elements is recommended. This crosstalk could be further suppressed by integrating a dielectric material between the two elements, which would provide increased thermal and electrical resistance. However, the presence of the dielectric would probably induce thermomechanical bending in the cantilever.

The most important characteristic for the piezoresistive element is deflection sensitivity. To test the piezoresistor, a precision three-axis microstage having 50 nm minimum increments was incorporated with a tungsten needle probe, a three-axis coarse manual stage, and a charge-coupled device (CCD) camera. The setup was similar to that used in [58]. While the needle probe deflected the microcantilever tip, resistance changes were recorded. The cantilever was mounted in a Wheatstone bridge. Since light intensity can change the resistance of the doped silicon, the intensity of the coaxial light source for the CCD was fixed during deflection sensitivity measurements.

The deflection sensitivities of the heater and the piezoresistor were measured, first under independent and then combined operation. Fig. 8(a) shows the voltage change in the piezoresistor as a function of the tip deflection where the applied voltage to the Wheatstone bridge was 2 V. When the piezoresistor was operated alone, its deflection sensitivity was $(4.25 \pm 0.05) \times 10^{-4}$ V/V $\cdot$ $\mu$m, which corresponded to a $\Delta R/R \cdot \mu$m sensitivity of $(17.0 \pm 0.2) \times 10^{-4}$. Since both the mechanical properties of the microcantilever and the piezoresistivity of the doped silicon can be modulated upon heating, it is important to understand the piezoresistor deflection sensitivity while the resistive heater is powered. Fig. 8(a) and (b) shows that the deflection sensitivity decreases as power dissipation in the heater increases. When the piezoresistor temperature increases due to the power input in the heater, the piezoresistive coefficients decrease [59]. In addition, the elastic modulus of the silicon decreases upon heating so that the cantilever becomes softer. For a given deflection, the soft cantilever will experience less stress change than the stiff cantilever. These two effects are combined and decrease the deflection sensitivity of the piezoresistor upon heating. Heating affects not only the deflection sensitivity but also the offset in the voltage output from the bridge. To measure the voltage offset upon heating, the tungsten needle probe was brought into contact with the microcantilever probe tip and the Wheatstone bridge was tuned to give zero output voltage. Then, the resistive heater was heated with a certain power and the voltage output from the bridge was measured without deflection. Fig. 8(c) shows that the voltage offset from the initially balanced Wheatstone bridge linearly increases with power dissipation in the heater.

It is typically assumed that microcantilever heaters having high-doped legs will have negligible piezoresistive effect [42],

TABLE I
SUMMARIZED BASIC CHARACTERIZATION RESULTS

| | Heater | Piezoresistor |
|---|---|---|
| Measured electrical resistance ($k\Omega$) | 0.466 ± 0.005 | 7.65 ± 0.04 |
| Simulated electrical resistance ($k\Omega$) | 0.57 | 8.60 |
| TCR ($\Omega/\Omega$-°C) | $(2.01 \pm 0.04) \times 10^{-3}$ | $(8.3 \pm 0.4) \times 10^{-4}$ |
| Deflection sensitivity (V/V-$\mu$m) | $(7.9 \pm 0.5) \times 10^{-5}$ | $(4.25 \pm 0.05) \times 10^{-4}$ |
| Spring constant (N/m) | 2.3 ± 0.2 | |
| Resonance frequency (kHz) | 73.0 ± 0.7 | |
| Quality factor | 118 ± 9 | |

since high-doped silicon has very low piezoresistivity [59]. In addition to low piezoresistivity in the high-doped legs, resistance in the legs which is 10% of the overall cantilever resistance at most [60], further suppresses the cantilever resistance change attributed to the cantilever deflection. If the cantilever leg resistance is negligible, the cantilever electrical resistance is dominated by temperature modulation. Little, if any, effort has been made to measure deflection sensitivity of microcantilever heaters while their vertical displacement sensitivity has been thoroughly investigated [29], [30]. The cantilever heater was configured in a second Wheatstone bridge set to 2 V and, the voltage output was measured, which is shown in Fig. 8(d). The deflection sensitivity of the heater obtained from the linear fit was $(7.9 \pm 0.5) \times 10^{-5}$ V/V $\cdot$ $\mu$m, which corresponded to a $\Delta R/R \cdot \mu$m sensitivity of $(3.2 \pm 0.2) \times 10^{-4}$.

Table I summarizes basic characterization results and includes simulated electrical resistances which show good agreement with the measurement. Characterized mechanical properties such as spring constant, resonance frequency, and quality factor are also included in Table I.

### B. Cantilever Topography Reading

It is expected that the piezoresistor deflection sensitivity will be the same for either a point deflection measurement or topography reading, since the piezoresistor is a strain sensor. The thermal signal from the cantilever heater can be used for topography mapping by measuring thermal conductance between the cantilever to the substrate [31], [32]. It is expected that the heater topography sensitivity will be much different from the heater deflection sensitivity. To test the topography sensitivity of the piezoresistor and the heater, the cantilever array was mounted in a commercial atomic force microscope (AFM) system (MFP-3D, Asylum research) to scan a calibration grating. The silicon grating had 200 nm mesas that were evenly spaced. The two Wheatstone bridges were interfaced with data acquisition inputs into the AFM controller.

When the cantilever deflected against the calibration grating, the resistance of the piezoresistor changes and this unbalanced the Wheatstone bridge configured for the piezoresistor (piezoresistive reading). When the gap distance between the cantilever heater and the substrate changed, the thermal resistance from the cantilever to the substrate was modulated. This modulation changed the cantilever temperature which was transduced into the voltage signal from the Wheatstone bridge configured for the heater (thermal reading). This thermal reading concept originates from thermomechanical data storage research [26] and detailed demonstrations in contact mode [31] and tapping mode [32] have recently been reported. Theoretical and experimental studies have been published to compare the sensitivity of piezoresistive and thermal sensing. However, previous work employed two similarly sized cantilevers that have either resistive heaters or piezoresistors in simulations [27] or experimented only on thermal reading, and then compared its sensitivity to previously reported sensitivities for piezoresistive reading [31]. The most relevant comparison could be performed on the same cantilever which enables both thermal and piezoresistive reading but this has not been reported.

While the cantilever scanned the grating with the proportional-integral feedback loop turned off (constant height mode or deflection mode), either the piezoresistive reading or the thermal reading was recorded. Fig. 9 shows the piezoresistive reading and the thermal reading when the bias voltages to each Wheatstone bridge were 4 and 5 V. The scan area was $30 \times 30$ $\mu$m$^2$, the scan rate was 1 Hz (1 scan line/s), and each frame had an image resolution of $256 \times 256$ pixels. When one doped resistor, either the piezoresistor or the heater, was powered, the other one was not used. The images on the left show filtered piezoresistive readings with 42.3 Hz cutoff frequency and 20 dB output gain. The images on the right show unfiltered thermal readings. When the same bias voltages were used, the signal was too low to be measured with our electronics and so the piezoresistor readings were filtered and amplified, although the cutoff frequency of 42.3 Hz could distort the signals. In contrast, thermal readings were sensitive enough not to require filtering or amplification. Piezoresistive signals linearly increased with the bias voltage to the Wheatstone bridge and the measured topography sensitivity was approximately $(2.57 \pm 0.05) \times 10^{-7}$ V/V $\cdot$ nm when the bias voltage was less than 6 V. The thermal topography sensing was much more sensitive than the piezoresistive sensing, as expected from previous publications [27], [31]. Thermal reading sensitivity ranged from $(1.00 \pm 0.05) \times 10^{-6}$ to $(5.89 \pm 0.04) \times 10^{-6}$ V/V $\cdot$ nm when the bias voltage changed from 3 to 6 V.

After the independent operation of each doped resistor was performed, both the piezoresistor and the heater were powered simultaneously when the cantilever scanned the same calibration grating. Fig. 10 shows the piezoresistive reading and the thermal reading when the bias voltages to each Wheatstone bridge were 4 and 5 V. The other scanning parameters remained unchanged. Again, the images on the left show filtered and amplified piezoresistive readings and the images on the right show unfiltered thermal readings. Thermal readings were similar and comparable to the results from the independent operation since the additional heating from the piezoresistor would not affect the resistive heater temperature. However, the piezoresistive readings were significantly different to the results in independent operation (Fig. 9). Their signals showed steep increase with the bias voltage so that the topography sensitivity was not constant any more. Moreover, the sensitivity increased rather than decreased with the bias voltage. This is

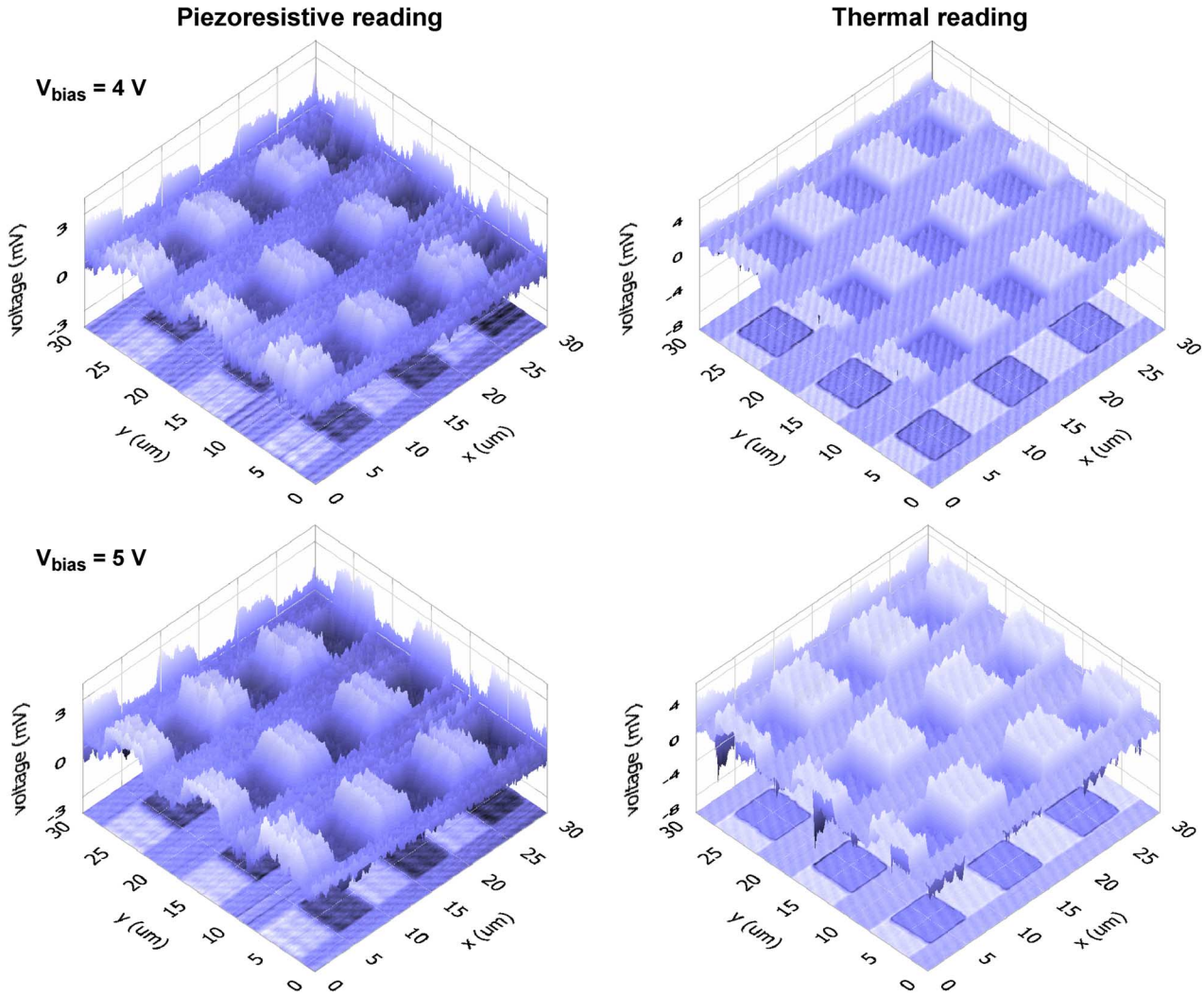


Fig. 9. Piezoresistive reading and thermal reading upon independent operation. Either the piezoresistor or the heater is operated independently. The left images show filtered piezoresistive reading with 20 dB gain and the right images show unfiltered thermal reading from a single cantilever. Bias voltages to each Wheatstone bridge are (top) 4 and (bottom) 5 V.

counterintuitive since Fig. 8 confirmed that the deflection sensitivity of the piezoresistor decreases as power dissipation in the heater increases. As mentioned above, the laser optical feedback was turned off during the scanning so that the cantilever deflection or contact force could not be controlled. Thus, the gap distance between the cantilever legs and the substrate may have varied significantly. When the power dissipation in the heater is sufficiently high enough to increase the temperature of the piezoresistor, the temperature change in the piezoresistor due to the gap distance modulation could be significant. The temperature change in the piezoresistor unbalances the Wheatstone bridge and signal because the temperature modulation exceeds the signal due to mechanical deflection. This is the most probable explanation for the enhanced piezoresistive readings when both the piezoresistor and the heater are powered. To confirm this, one cantilever in the array scanned the grating in a constant force mode with optical feedback while both the piezoresistor and the heater were powered. Output from the piezoresistor was similar in magnitude to results in Fig. 10 and increased with the bias voltage. Since there was no additional strain in the piezoresistor after the cantilever engaged the grating in a constant force mode, output from the piezoresistor was only due to its temperature modulation via air gap change during scanning.

Fig. 11 summarizes the topography sensitivity results for comparison between the piezoresistive reading and the thermal reading for both independent and combined operation. Even though the piezoresistor was designed to transduce mechanical strain into a measurable electrical signal, it could be better to use it as a thermal displacement sensor when the temperature of the piezoresistor is sufficiently high. Interestingly, the topography sensitivity of the piezoresistive reading might exceed that of the thermal reading at bias voltages above 6 V. Since we have fully characterized the heater and the piezoresistor for both independent and combined operation, both elements can be used simultaneously even though this is not our primary interest. Temperature rise in the piezoresistors during heater operation cannot be circumvented so that higher doping concentration for piezoresistors is recommended to reduce temperature dependence of piezoresistive coefficients for applications requiring simultaneous heater and piezoresistor operation. However, higher doping results in reduced piezoresistive coefficients.

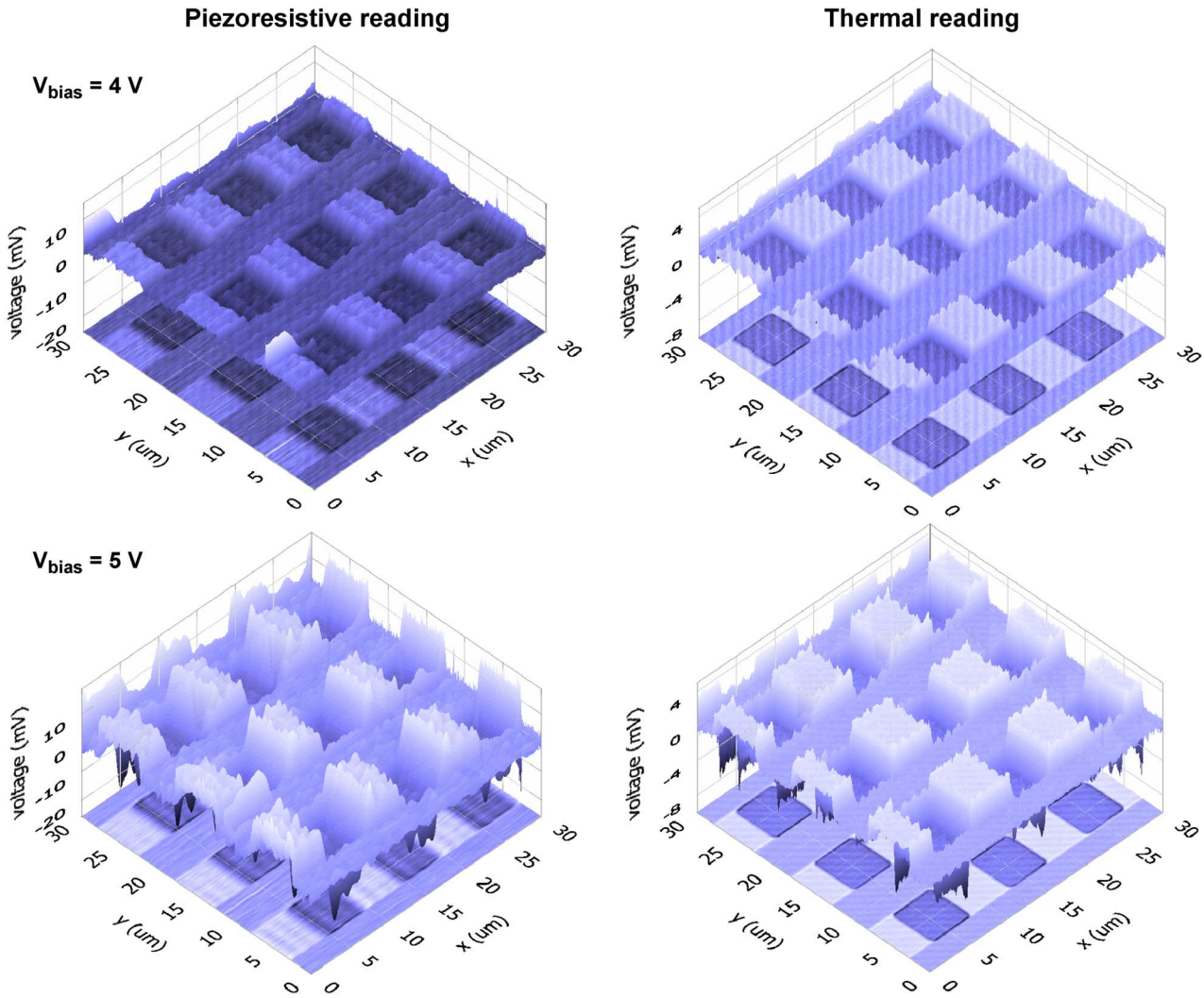


Fig. 10. Piezoresistive reading and thermal reading upon combined operation. Both the piezoresistor and the heater are operated simultaneously. The left images show filtered piezoresistive reading with 20 dB gain and the right images show unfiltered thermal reading from a single cantilever. Bias voltages to the two Wheatstone bridges are (top) 4 and (bottom) 5 V.

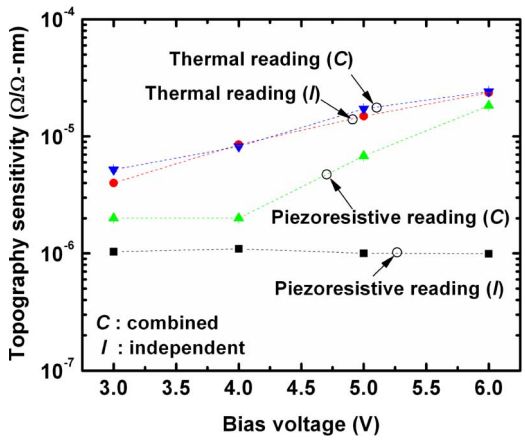


Fig. 11. Topography sensitivity comparison between piezoresistive reading and thermal reading for both independent and combined operation.

Noise measurements were performed for both the piezoresistor and the heater using a low noise preamplifier (SR560, Stanford research systems) and a spectrum analyzer (SR770, Stanford research systems). Using measured noise spectra and topographic sensitivities, noise-limited resolutions were directly calculated (Resolution = Noise/Sensitivity). Table II summarizes sensitivity, noise, and resolution for tested bias voltages. Thermal reading is superior to piezoresistive reading in terms of minimum detectable topographic change. With 3 V bias to each Wheatstone bridge, noise-limited resolutions of thermal reading and piezoresistive reading were $0.46 \pm 0.03$ and $3.4 \pm 0.4$ nm$/\sqrt{\text{Hz}}$, respectively. Resolution was improved as the bias voltage increased since sensitivity enhancement far exceeded noise increase for the voltage range tested. It is expected that resolution would be constant or reduced at higher bias voltages. The comparison is not necessarily a fair one due to their differences in sensing mechanism, size, resistance, and power consumption. Nevertheless, thermal reading senses the change in displacement but piezoresistive reading senses the change in cantilever deflection. Thus, thermal reading is applicable without contact to the substrate while piezoresistive reading is only possible with contact to the substrate.

TABLE II
SENSITIVITY, NOISE, AND RESOLUTION OF THE HEATER AND THE PIEZORESISTOR DURING INDEPENDENT OPERATION

| | | 3 V | 4 V | 5 V | 6 V |
|---|---|---|---|---|---|
| Heater | Sensitivity ($\mu$V/nm) | 3.0 ± 0.2 | 8.4 ± 0.2 | 18.5 ± 0.2 | 35.4 ± 0.2 |
| | Noise ($\mu$V/$\sqrt{\text{Hz}}$) | 1.39 ± 0.07 | 1.64 ± 0.08 | 1.80 ± 0.09 | 2.1 ± 0.1 |
| | Resolution (nm/$\sqrt{\text{Hz}}$) | 0.46 ± 0.03 | 0.19 ± 0.01 | 0.097 ± 0.005 | 0.058 ± 0.003 |
| Piezoresistor | Sensitivity ($\mu$V/nm) | 0.77 ± 0.02 | 1.09 ± 0.02 | 1.25 ± 0.03 | 1.50 ± 0.02 |
| | Noise ($\mu$V/$\sqrt{\text{Hz}}$) | 2.7 ± 0.3 | 2.7 ± 0.3 | 3.0 ± 0.3 | 3.0 ± 0.3 |
| | Resolution (nm/$\sqrt{\text{Hz}}$) | 3.4 ± 0.4 | 2.5 ± 0.3 | 2.4 ± 0.2 | 2.0 ± 0.2 |

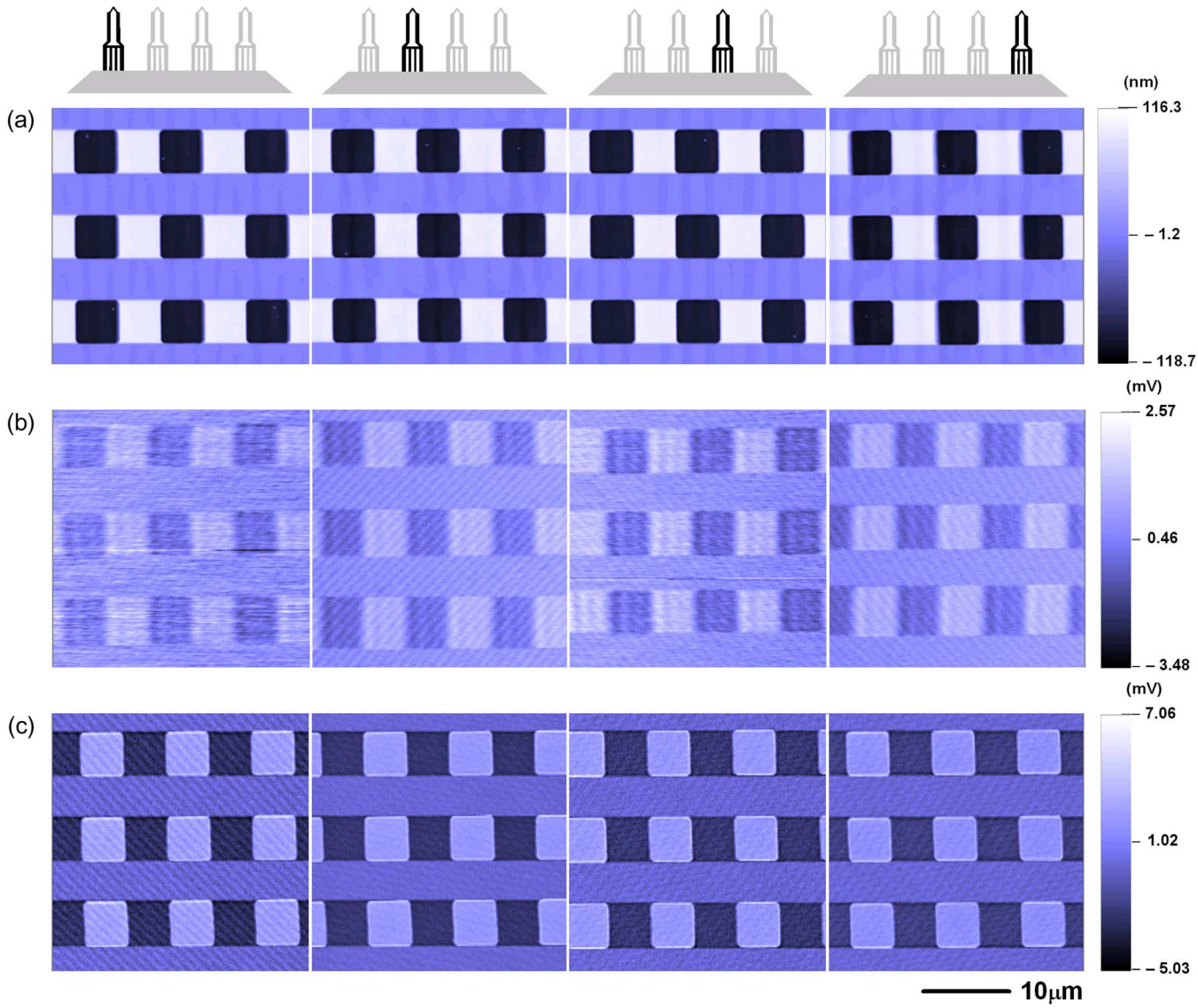


Fig. 12. (a) Optical lever topography, (b) filtered piezoresistive reading with 20 dB gain, and (c) unfiltered thermal reading. Images on each column are obtained from each cantilever in the given array. After obtaining optical lever topography, all four cantilevers are operated simultaneously but either the piezoresistor or the heater in a cantilever is operated at a time with 4 V bias voltage.

### C. Array Characterization

Since all cantilevers in an array chip were fabricated adjacent to each other, their dimensions including the cantilever thickness were more or less identical. Local variations during fabrication was not likely to exist within the area of one array. The most relevant array characterization would be to scan the calibration grating using four cantilevers at the same time.

Fig. 12 shows the topography based on scans performed with optical reading, piezoresistive reading and thermal reading for four cantilevers in a single array chip. Four cantilevers were operated simultaneously but either the piezoresistor or the heater in a cantilever was powered at a time. The bias voltage was fixed at 4 V for both Wheatstone bridges. Before the array chip was attached and wire-bonded to the custom PCB, it was mounted on the dedicated cantilever holder in the commercial AFM. This enabled topography scans employing a laser and a photodiode. The images on the first row show the topography data from the four cantilevers. This topography was not necessary since the cantilevers have two additional topography sensing mechanisms. However, the obtained four topographic images could be used to compare the tip shape of each cantilever. The second and third rows of the images show results from the filtered piezoresistive reading and the unfiltered thermal reading, respectively. The measured sensitivities for the piezoresistive reading ranged from $(1.50 \pm 0.04) \times 10^{-7}$ to $(1.61 \pm 0.05) \times 10^{-7}$ V/V $\cdot$ nm and the sensitivities for the thermal reading ranged from $(4.80 \pm 0.06) \times 10^{-6}$ to $(6.00 \pm 0.09) \times 10^{-6}$ V/V $\cdot$ nm.

Most of the tests on the calibration grating except for the topography relying on the optical readout contained significant noise in their images. The major sources were 60 Hz and its harmonics from the power electronics and laboratory environment. More effort should follow to suppress them. Moreover, both the piezoresistive reading and the thermal reading were performed without any feedback control so that their signal readouts possibly contained abnormal spikes when the cantilever encountered a sudden change in local topography. Since both the piezoresistive reading and the thermal reading can be used for a feedback loop, it is recommended to construct a feedback control to eliminate the parasitic spikes and also prevent mechanical wear problems of the probe tip.

## IV. Summary and Conclusion

This paper describes the design, fabrication, and characterization of improved all-silicon microcantilever heaters with integrated piezoresistors. Instead of using metal traces, only doped silicon was used to suppress parasitic bending and prevent electromigration upon heating. Electrical and thermal crosstalks between the heater and the piezoresistor were thoroughly investigated and sensitivity comparison for the two topographic sensors embedded in a single cantilever was demonstrated for the first time. The fabricated microcantilevers exhibited successful integration of a resistive heater with a piezoresistive element in each cantilever and four cantilevers were arrayed for parallel operations. In addition to individual cantilever characterization, array characterization was also performed on a calibration grating. The fabricated microcantilever array will be applicable to parallel scanning probe lithography and force spectroscopy. A compact customized AFM system could be constructed with either the heater or the piezoresistor. The results obtained in this paper will give guidelines for the fabrication and integration of large 1-D or 2-D arrays of multifunctional microcantilevers.

## References


[1] T. R. Albrecht and C. F. Quate, "Atomic resolution imaging of a nonconductor by atomic force microscopy," *J. Appl. Phys.*, vol. 62, no. 7, pp. 2599–2602, Oct. 1987.

[2] N. V. Lavrik and P. G. Datskos, "Femtogram mass detection using photothermally actuated nanomechanical resonators," *Appl. Phys. Lett.*, vol. 82, no. 16, pp. 2697–2699, 2003.

[3] M. Lutwyche, C. Andreoli, G. Binnig, J. Brugger, U. Drechsler, W. Häberle, H. Rohrer, H. Rothuizen, P. Vettiger, G. Yaralioglu, and C. Quate, "5 × 5 2D AFM cantilever arrays a first step towards a Terabit storage device," *Sens. Actuators A, Phys.*, vol. 73, no. 1/2, pp. 89–94, Mar. 1999.

[4] P. Vettiger, J. Brugger, M. Despont, U. Drechsler, U. Dürig, W. Häberle, M. Lutwyche, H. Rothuizen, R. Stutz, R. Widmer, and G. Binnig, "Ultrahigh density, high-data-rate NEMS-based AFM data storage system," *Microelectron. Eng.*, vol. 46, no. 1, pp. 11–17, May 1999.

[5] M. Despont, J. Brugger, U. Drechsler, U. Dürig, W. Häberle, M. Lutwyche, H. Rothuizen, R. Stutz, R. Widmer, G. Binnig, H. Rohrer, and P. Vettiger, "VLSI-NEMS chip for parallel AFM data storage," *Sens. Actuators A, Phys.*, vol. 80, no. 2, pp. 100–107, Mar. 2000.

[6] U. Dürig, G. Cross, M. Despont, U. Drechsler, W. Häberle, M. I. Lutwyche, H. Rothuizen, R. Stutz, R. Widmer, P. Vettiger, G. K. Binnig, W. P. King, and K. E. Goodson, "'Millipede'—An AFM data storage system at the frontier of nanotribology," *Tribol. Lett.*, vol. 9, no. 1/2, pp. 25–32, Dec. 2000.

[7] P. Vettiger, G. Cross, M. Despont, U. Drechsler, U. Dürig, B. Gotsmann, W. Häberle, M. Lantz, H. Rothuizen, R. Stutz, and G. Binnig, "The 'Millipede'—Nanotechnology entering data storage," *IEEE Trans. Nanotechnol.*, vol. 1, no. 1, pp. 39–55, Mar. 2002.

[8] S. C. Minne, S. R. Manalis, A. Atalar, and C. F. Quate, "Independent parallel lithography using the atomic force microscope," *J. Vac. Sci. Technol. B, Microelectron. Process. Phenom.*, vol. 14, no. 4, pp. 2456–2461, Jul. 1996.

[9] X. Wang and C. Liu, "Multifunctional probe array for nano patterning and imaging," *Nano Lett.*, vol. 5, no. 10, pp. 1867–1872, Oct. 2005.

[10] S. C. Minne, G. Yaralioglu, S. R. Manalis, J. D. Adams, J. Zesch, A. Atalar, and C. F. Quate, "Automated parallel high-speed atomic force microscopy," *Appl. Phys. Lett.*, vol. 72, no. 18, pp. 2340–2342, 1998.

[11] L. Aeschimann, A. Meister, T. Akiyama, B. W. Chui, P. Niedermann, H. Heinzelmann, N. F. De Rooij, U. Staufer, and P. Vettiger, "Scanning probe arrays for life sciences and nanobiology applications," *Microelectron. Eng.*, vol. 83, no. 4–9, pp. 1698–1701, Apr.–Sep. 2006.

[12] M. Despont, T. Altebaeumer, P. Bächtold, G. K. Binnig, G. Cherubini, U. Drechsler, U. Dürig, E. Eleftheriou, B. Gotsmann, W. Häberle, C. Hableitner, D. Jubin, A. Knoll, M. A. Lantz, A. Pantazi, H. Pozidis, H. Rothuizen, A. Sebastian, R. Stutz, P. Vettiger, D. Wiesmann, and J. Windeln, "A highly parallel probe-based storage system," in *Proc. Dig. Papers—Microprocess. Nanotechnol.*, 2004, pp. 4–5.

[13] M. Despont, U. Drechsler, R. Yu, H. B. Pogge, and P. Vettiger, "Wafer-scale microdevice transfer/interconnect: Its application in an AFM-based data-storage system," *J. Microelectromech. Syst.*, vol. 13, no. 6, pp. 895–901, Dec. 2004.

[14] Y. S. Kim, C. S. Lee, W. H. Jin, S. Jang, H. J. Nam, and J. U. Bu, "100 × 100 thermo-piezoelectric cantilever array for SPM nano-data-storage application," *Sens. Mater.*, vol. 17, no. 2, pp. 57–63, 2005.

[15] K. Salaita, Y. H. Wang, J. Fragala, R. A. Vega, C. Liu, and C. A. Mirkin, "Massively parallel dip-pen nanolithography with 55 000-pen two-dimensional arrays," *Angew. Chem.*, vol. 45, no. 43, pp. 7220–7223, 2006.

[16] J. Fritz, M. K. Baller, H. P. Lang, H. Rothuizen, P. Vettiger, E. Meyer, H. J. Güntherodt, C. Gerber, and J. K. Gimzewski, "Translating biomolecular recognition into nanomechanics," *Science*, vol. 288, no. 5464, pp. 316–318, Apr. 2000.

[17] M. K. Baller, H. P. Lang, J. Fritz, C. Gerber, J. K. Gimzewski, U. Drechsler, H. Rothuizen, M. Despont, P. Vettiger, F. M. Battiston, J. P. Ramseyer, P. Fornaro, E. Meyer, and H. J. Güntherodt, "A cantilever array-based artificial nose," *Ultramicroscopy*, vol. 82, no. 1–4, pp. 1–9, Feb. 2000.

[18] F. M. Battiston, J. P. Ramseyer, H. P. Lang, M. K. Baller, C. Gerber, J. K. Gimzewski, E. Meyer, and H. J. Güntherodt, "A chemical sensor based on a microfabricated cantilever array with simultaneous resonance-frequency and bending readout," *Sens. Actuators B, Chem.*, vol. 77, no. 1/2, pp. 122–131, Jun. 2001.

[19] G. H. Wu, R. H. Datar, K. M. Hansen, T. Thundat, R. J. Cote, and A. Majumdar, "Bioassay of prostate-specific antigen (PSA) using microcantilevers," *Nat. Biotechnol.*, vol. 19, no. 9, pp. 856–860, 2001.

[20] Y. Arntz, J. D. Seelig, H. P. Lang, J. Zhang, P. Hunziker, J. P. Ramseyer, E. Meyer, M. Hegner, and C. Gerber, "Label-free protein assay based on a nanomechanical cantilever array," *Nanotechnology*, vol. 14, no. 1, pp. 86–90, 2003.

[21] F. Huber, M. Hegner, C. Gerber, H. J. Güntherodt, and H. P. Lang, "Label free analysis of transcription factors using microcantilever arrays," *Biosens. Bioelectron.*, vol. 21, no. 8, pp. 1599–1605, Feb. 2006.

[22] S. L. Biswal, D. Raorane, A. Chaiken, and A. Majumdar, "Using a microcantilever array for detecting phase transitions and stability of DNA," *J. Assoc. Lab. Autom.*, vol. 11, no. 4, pp. 222–226, 2006.

[23] Z. X. Yang, Y. Yu, X. X. Li, and H. F. Bao, "Nano-mechanical electrothermal probe array used for high-density storage based on NEMS technology," *Microelectron. Reliab.*, vol. 46, no. 5/6, pp. 805–810, May/Jun. 2006.

[24] S. A. Miller, K. L. Turner, and N. C. MacDonald, "Microelectromechanical scanning probe instruments for array architectures," *Rev. Sci. Instrum.*, vol. 68, no. 11, pp. 4155–4162, Nov. 1997.

[25] M. Tortonese, R. C. Barrett, and C. F. Quate, "Atomic resolution with an atomic force microscope using piezoresistive detection," *Appl. Phys. Lett.*, vol. 62, no. 8, pp. 834–836, Feb. 1993.

[26] G. Binnig, M. Despont, U. Drechsler, W. Häberle, M. Lutwyche, P. Vettiger, H. J. Mamin, B. W. Chui, and T. W. Kenny, "Ultrahigh-density atomic force microscopy data storage with erase capability," *Appl. Phys. Lett.*, vol. 74, no. 9, pp. 1329–1331, Mar. 1999.

[27] W. P. King, T. W. Kenny, and K. E. Goodson, "Comparison of thermal and piezoresistive sensing approaches for atomic force microscopy topography measurements," *Appl. Phys. Lett.*, vol. 85, no. 11, pp. 2086–2088, Sep. 2004.

[28] W. P. King, "Design analysis of heated atomic force microscope cantilevers for nanotopography measurements," *J. Micromech. Microeng.*, vol. 15, no. 12, pp. 2441–2448, Dec. 2005.

[29] U. Dürig, "Fundamentals of micromechanical thermoelectric sensors," *J. Appl. Phys.*, vol. 98, no. 4, p. 044 906, 2005.

[30] M. A. Lantz, G. K. Binnig, M. Despont, and U. Drechsler, "A micromechanical thermal displacement sensor with nanometre resolution," *Nanotechnology*, vol. 16, no. 8, pp. 1089–1094, Aug. 2005.

[31] K. J. Kim, K. Park, J. Lee, Z. M. Zhang, and W. P. King, "Nanotopographical imaging using a heated atomic force microscope cantilever probe," *Sens. Actuators A, Phys.*, vol. 136, no. 1, pp. 95–103, May 2007.

[32] K. Park, J. Lee, Z. M. Zhang, and W. P. King, "Nanotopographical imaging with a heated atomic force microscope cantilever in tapping mode," *Rev. Sci. Instrum.*, vol. 78, p. 043 709, 2007.

[33] Z. X. Yang, X. X. Li, Y. L. Wang, H. F. Bao, and M. Liu, "Micro cantilever probe array integrated with Piezoresistive sensor," *Microelectron. J.*, vol. 35, no. 5, pp. 479–483, May 2004.

[34] N. Abedinov, P. Grabiec, T. Gotszalk, T. Ivanov, J. Voigt, and I. W. Rangelow, "Micromachined piezoresistive cantilever array with integrated resistive microheater for calorimetry and mass detection," *J. Vac. Sci. Technol. A, Vac. Surf. Films*, vol. 19, no. 6, pp. 2884–2888, Nov. 2001.

[35] B. A. Nelson, W. P. King, A. Laracuente, P. E. Sheehan, and L. J. Whitman, "Direct deposition of continuous metal nanostructures by thermal dip-pen nanolithography," *Appl. Phys. Lett.*, vol. 88, no. 3, p. 033 104, 2006.

[36] B. Gotsmann, U. Dürig, J. Frommer, and C. J. Hawker, "Exploiting chemical switching in a Diels-Alder polymer for nanoscale probe lithography and data storage," *Adv. Funct. Mater.*, vol. 16, no. 11, pp. 1499–1505, 2006.

[37] E. O. Sunden, T. L. Wright, J. Lee, S. A. Graham, and W. P. King, "Room temperature chemical vapor deposition and mass detection on a heated atomic force microscope cantilever," *Appl. Phys. Lett.*, vol. 88, no. 3, p. 033 107, 2006.

[38] R. Szoszkiewicz, T. Okada, S. C. Jones, T. D. Li, W. P. King, S. R. Marder, and E. Riedo, "High-speed, sub-15 nm feature size thermochemical nanolithography," *Nano Lett.*, vol. 7, no. 4, pp. 1064–1069, 2007.

[39] T. Arai and M. Tomitori, "Removal of contamination and oxide layers from UHV-AFM tips," *Appl. Phys. A, Solids Surf.*, vol. 66, no. S1, pp. S319–S323, 1998.

[40] M. Tomitori and T. Arai, "Tip cleaning and sharpening processes for noncontact atomic force microscope in ultrahigh vacuum," *Appl. Surf. Sci.*, vol. 140, no. 3, pp. 432–438, Feb. 1999.

[41] S. L. Biswal, D. Raorane, A. Chaiken, H. Birecki, and A. Majumdar, "Nanomechanical detection of DNA melting on microcantilever surfaces," *Anal. Chem.*, vol. 78, no. 20, pp. 7104–7109, 2006.

[42] J. Lee, T. Beechem, T. L. Wright, B. A. Nelson, S. Graham, and W. P. King, "Electrical, thermal, and mechanical characterization of silicon microcantilever heaters," *J. Microelectromech. Syst.*, vol. 15, no. 6, pp. 1644–1655, Dec. 2006.

[43] J. R. Black, "Electromigration—A brief survey and some recent results," *IEEE Trans. Electron Devices*, vol. ED-16, no. 4, pp. 338–347, Apr. 1969.

[44] C. Liu, *Foundations of MEMS*. Upper Saddle River, NJ: Pearson, 2006.

[45] X. Yu, D. Zhang, W. Wang, and T. Li, "A sensor platform based on piezoresistive cantilever," in *Proc. IEEE Conf. Electron Devices, Solid-State Circuits*, 2003, pp. 121–124.

[46] J. A. Harley and T. W. Kenny, "1/F noise considerations for the design and process optimization of piezoresistive cantilevers," *J. Microelectromech. Syst.*, vol. 9, no. 2, pp. 226–235, Jun. 2000.

[47] T. L. Wright, "Design and fabrication of heated atomic force microscope cantilevers," M.S. thesis, Woodruff School Mech. Eng., Georgia Inst. Technol., Atlanta, GA, 2005.

[48] B. W. Chui, T. W. Kenny, H. J. Mamin, B. D. Terris, and D. Rugar, "Independent detection of vertical and lateral forces with a sidewall-implanted dual-axis piezoresistive cantilever," *Appl. Phys. Lett.*, vol. 72, no. 11, pp. 1388–1390, Mar. 1998.

[49] X. M. Yu, J. Thaysen, O. Hansen, and A. Boisen, "Optimization of sensitivity and noise in piezoresistive cantilevers," *J. Appl. Phys.*, vol. 92, no. 10, pp. 6296–6301, Nov. 2002.

[50] S. Reggiani, M. Valdinoci, L. Colalongo, M. Rudan, G. Baccarani, A. D. Stricker, F. Illien, N. Felber, W. Fichtner, and L. Zullino, "Electron and hole mobility in silicon at large operating temperatures—Part I: Bulk mobility," *IEEE Trans. Electron Devices*, vol. 49, no. 3, pp. 490–499, Mar. 2002.

[51] S. D. Senturia, *Microsystem Design*. Boston, MA: Kluwer, 2001.

[52] B. W. Chui, T. D. Stowe, Y. S. Ju, K. E. Goodson, T. W. Kenny, H. J. Mamin, B. D. Terris, and R. P. Ried, "Low-stiffness silicon cantilever with integrated heaters and piezoresistive sensors for high-density AFM thermomechanical data storage," *J. Microelectromech. Syst.*, vol. 7, no. 1, pp. 69–78, Mar. 1998.

[53] B. W. Chui, M. Asheghi, Y. S. Ju, K. E. Goodson, T. W. Kenny, and H. J. Mamin, "Intrinsic-carrier thermal runaway in silicon microcantilevers," *Microscale Thermophys. Eng.*, vol. 3, no. 3, pp. 217–228, Jul. 1999.

[54] M. Kuball, J. M. Hayes, M. J. Uren, T. Martin, J. C. H. Birbeck, R. S. Balmer, and B. T. Hughes, "Measurement of temperature in active high-power AlGaN/GaN HFETs using Raman spectroscopy," *IEEE Electron Device Lett.*, vol. 23, no. 1, pp. 7–9, Jan. 2002.

[55] M. Kuball, S. Rajasingam, A. Sarua, M. J. Uren, T. Martin, B. T. Hughes, K. P. Hilton, and R. S. Balmer, "Measurement of temperature distribution in multifinger AlGaN/GaN heterostructure field-effect transistors using micro-Raman spectroscopy," *Appl. Phys. Lett.*, vol. 82, no. 1, pp. 124–126, Jan. 2003.

[56] R. Diffenderfer, *Electronic Devices: Systems and Applications*. Clifton Park, NY: Thomson/Delmar, 2005.

[57] J. Lee and W. P. King, "Microcantilever hotplates: Design, fabrication, and characterization," *Sens. Actuators A, Phys.*, vol. 136, no. 1, pp. 291–298, May 2007.

[58] B. W. Chui, L. Aeschimann, T. Akiyama, U. Staufer, N. F. de Rooij, J. Lee, F. Goericke, W. P. King, and P. Vettiger, "Advanced temperature compensation for piezoresistive cantilevers using 45-degree angle resistor pairs," *Rev. Sci. Instrum.*, vol. 78, p. 043 706, 2007.

[59] R. Hull, *Properties of Crystalline Silicon*. London, U.K.: INSPEC, 1999.

[60] J. Lee, T. L. Wright, M. R. Abel, E. O. Sunden, A. Marchenkov, S. Graham, and W. P. King, "Thermal conduction from microcantilever heaters in partial vacuum," *J. Appl. Phys.*, vol. 101, no. 1, p. 014 906, Jan. 2007.

**Jungchul Lee** received the B.S. and M.S. degrees in mechanical engineering from Seoul National University, Seoul, Korea, in 2001 and 2003, respectively, and the Ph.D. degree in mechanical engineering from Georgia Institute of Technology, Atlanta, in 2007.

He is currently a Postdoctoral Research Associate at the University of Illinois at Urbana–Champaign, Urbana. His research focuses on developing microcantilever sensors for scanning probe microscopy and bio/chemical sensing.

**William P. King** received the B.S. degree in mechanical engineering from the University of Dayton, Dayton, OH, in 1996, and the M.S. and Ph.D. degrees in mechanical engineering from Stanford University, Stanford, CA, in 1998 and 2002, respectively.

He is Associate Professor and Kritzer Faculty Scholar in the Department of Mechanical Science and Engineering, University of Illinois at Urbana–Champaign (UIUC), Urbana. During 1999 through 2001, he spent 16 months in the Micro/NanoMechanics Group of the IBM Zurich Research Laboratory. During the years 2002 through 2006, he was on the faculty at Georgia Institute of Technology. At UIUC, his group works on thermal engineering of micro/nanomechanical devices, nanomanufacturing, and thermal processing.

Dr. King is the winner of the CAREER award from the National Science Foundation (2003), the Presidential Early Career Award for Scientists and Engineers award from the Department of Energy (2005), and the Young Investigator Award from the Office of Naval Research (2007). In 2006, *Technology Review Magazine* named him to the TR35—one of the people under the age of 35 whose innovations are likely to change the world. In 2007, his innovations were selected for an R&D 100 Award and a Micro/Nano 25 Award. He sits on the advisory board at several companies and is a Fellow of the Defense Sciences Research Council.